Bone 185 (2024) 117132

Contents lists available at ScienceDirect

Bone

journal homepage: www.elsevier.com/locate/bone

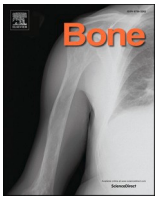

Full Length Article

PGC-1α/LDHA signaling facilitates glycolysis initiation to regulate mechanically induced bone remodeling under inflammatory microenvironment

Jiani Liu, Jixiao Wang, Ziyao Wang, Huiying Ren, Zijie Zhang, Yajing Fu, Lan Li, Zhiyuan Shen, Tianyi Li, Shuai Tang, Fulan Wei *

Department of Orthodontics, School and Hospital of Stomatology, Cheeloo College of Medicine, Shandong University & Shandong Key Laboratory of Oral Tissue Regeneration & Shandong Engineering Research Center of Dental Materials and Oral Tissue Regeneration & Shandong Provincial Clinical Research Center for Oral Diseases, Jinan 250012, Shandong, China

ARTICLE INFO

Keywords:
Inflammation
Mechanical force
Bone remodeling
Glucose metabolism
PGC-1α
LDHA

ABSTRACT

The mechanosensitivity of inflammation can alter cellular mechanotransduction. However, the underlying mechanism remains unclear. This study aims to investigate the metabolic mechanism of inflammation under mechanical force to guide tissue remodeling better. Herein, we found that inflammation hindered bone remodeling under mechanical force, accompanied by a simultaneous enhancement of oxidative phosphorylation (OXPHOS) and glycolysis. The control of metabolism direction through GNE-140 and Visomitin revealed that enhanced glycolysis might act as a compensatory mechanism to resist OXPHOS-induced osteoclastogenesis by promoting osteogenesis. The inhibited osteogenesis induced by inflammatory mechanical stimuli was concomitant with a reduced expression of peroxisome proliferator-activated receptor gamma coactivator 1-alpha (PGC-1α). PGC-1α knockdown impeded osteogenesis under mechanical force and facilitated osteoclastogenesis by enhancing OXPHOS. Conversely, PGC-1α overexpression attenuated the impairment of bone remodeling by inflammatory mechanical signals through promoting glycolysis. This process benefited from the PGC-1α regulation on the transcriptional and translational activity of lactate dehydrogenase A (LDHA) and the tight control of the extracellular acidic environment. Additionally, the increased binding between PGC-1α and LDHA proteins might contribute to the glycolysis promotion within the inflammatory mechanical environment. Notably, LDHA suppression effectively eliminated the bone repair effect mediated by PGC-1α overexpression within inflammatory mechanical environments. In conclusion, this study demonstrated a novel molecular mechanism illustrating how inflammation orchestrated glucose metabolism through glycolysis and OXPHOS to affect mechanically induced bone remodeling.

1. Introduction

Inflammation is intimately linked to the development of most diseases [1,2]. Characterized by temporal and spatial heterogeneity [3], the dynamic response of inflammation is closely intertwined with mechanical force. Apart from extrinsic mechanical stimuli such as weight-bearing and friction at the site of inflammation [4,5], blood/interstitial flow, traction of cell-matrix interaction, and intercellular contacts all subject inflammatory cells to strong fluctuations in mechanical forces [6]. Homeostatic remodeling during inflammation makes cells more sensitive to mechanical stimuli [7]. This heightened sensitivity can lead to overloading of the original mechanical force and affect tissue remodeling through mechanotransduction alterations [8,9]. The influence of inflammation on mechanotransduction involves multiple factors such as ion channels [10], molecular pathways [11], and extracellular vesicles [12]. The execution of these activities necessitates energy metabolism for their maintenance. Interestingly, metabolism is also involved in aberrant mechanotransduction. The inflammatory mechanical environment induces changes in oxygen concentration and nutrient abundance, leading to metabolic reprogramming [13]. However, the potential mechanisms by which inflammatory mechanical signals affect tissue remodeling through metabolic reprogramming

* Corresponding author at: No.44-1 Wenhua Road West, 250012 Jinan, Shandong, China.
E-mail address: weifl@email.sdu.edu.cn (F. Wei).

https://doi.org/10.1016/j.bone.2024.117132
Received 8 January 2024; Received in revised form 29 April 2024; Accepted 20 May 2024
Available online 22 May 2024

remain to be elucidated.

Increasing glucose uptake and enhancing anaerobic glycolysis as the major source of adenosine triphosphate is a significant metabolic characteristic of cellular response to inflammatory mechanical stimuli [14]. This metabolic shift may stem from the activation of mitochondrial autophagy [15] and the coupling of actin with glycolytic enzymes [16]. In addition, inflammatory mechanical signals promote the enrichment of OXPHOS genes [17]. The modulation of metabolic fluxes in glycolysis and OXPHOS is pivotal in the glucose metabolic reprogramming that underlies the biological function of stem cells [18]. These metabolic adaptations effectively meet the energy demands and facilitate macromolecule synthesis during tissue remodeling [19]. Additionally, the metabolic intermediates regulate epigenetic modifications [20], communication between mitochondria and the nucleus [21], and receptor binding [22] to affect cell growth, development, pluripotency maintenance, and response to cellular stress. Therefore, we hypothesize that inflammatory mechanical stimuli can impact tissue remodeling through glucose metabolic reprogramming. PGC-1α plays a crucial role in gluconeogenesis and the preservation of glucose metabolic homeostasis across various organs [23,24]. It possesses the ability to sense intracellular AMP/ATP ratio changes, thereby governing glucose transportation, electron respiratory chain transmission, and oxidative stress [25]. Nevertheless, how PGC-1α orchestrates glucose metabolism to affect tissue remodeling in an inflammatory mechanical environment remains unclear.

Orthodontic treatment of periodontitis is considered as a representative model for studying the impacts of inflammatory mechanical stimuli. Periodontitis is characterized by periodontal tissues destruction and alveolar bone resorption, which can cause malocclusion and occlusal trauma that necessitate correction through orthodontic force [26]. As major periodontal osteoprogenitors implicated in orthodontic bone remodeling in periodontitis, periodontal ligament stem cells (PDLSCs) and bone marrow stromal cells (BMSCs) possess the ability to perceive and respond to periodontal microenvironment stimuli [27]. They convert mechanical stimuli into chemical signals, thereby facilitating anaerobic oxidation [15] and lactate release to regulate alveolar bone remodeling [28]. Exploring the role of glucose metabolism in orthodontic bone remodeling of periodontitis will shed light on the unique characteristics of tissue remodeling in this population. Furthermore, it can provide valuable insights into the metabolic mechanisms underlying the pathogenesis of inflammatory disorders within mechanical environments.

Hence, the present study aims to clarify how periodontitis affects mechanically induced alveolar bone remodeling through glucose metabolic reprogramming and the underlying molecular mechanisms. Our findings indicate that the impaired bone remodeling by inflammatory mechanical stimuli is accompanied by a dual enhancement of glycolysis and OXPHOS. Notably, the upregulation of glycolysis serves as a compensatory mechanism, promoting osteogenesis to counteract the osteoclast promoting induced by the heightened OXPHOS. During this process, OXPHOS-sensitive PGC-1α alters the direction of glucose metabolism by regulating the transcription, translation, and metabolite activity of LDHA, a crucial rate-limiting enzyme in glycolysis, thereby affecting mechanically induced bone remodeling. These findings contribute to our understanding of the metabolic dynamics underlying tissue remodeling in inflammatory mechanical microenvironments. Moreover, these results offer potential metabolic therapeutic strategies for tissue remodeling in inflammatory diseases within mechanical environments.

2. Results

2.1. Inflammatory microenvironment impaired the bone remodeling of periodontium under mechanical force

Obtained periodontal osteoprogenitors were identified through flow cytometry (Additional file 1: Fig. S1A, D). Alkaline phosphatase (ALP) staining (Additional file 1: Fig. S1B, E) and oil red O staining (Additional file 1: Fig. S1C, F) confirmed prolonged inflammatory induction with 10 ng/ml TNF-α could impair the osteogenic and lipogenic differentiation potential of the two cells. This was consistent with the characterization of periodontal tissues obtained from periodontitis donors [7,29]. Considering the higher levels of inflammatory factors and the restricted availability of periodontal osteoprogenitors even in the stable periods of periodontitis [30], 10 ng/ml TNF-α was chosen as an alternative method of inflammatory induction for further studies [31].

After 12-h and 24-h mechanotransduction, the osteogenic differentiation potential of periodontal osteoprogenitors in each group was evaluated (Fig. 1A). The inflammatory microenvironment exhibited decreased expression of osteogenesis-related genes and proteins (Fig. 1B-G; Additional file 1: Fig. S2A, B). Correspondingly, the osteoclast-related genes were increased with inflammatory treatment (Fig. 1B, C; Additional file 1: Fig. S2A, B). Additionally, flow cytometric analysis (Additional file 1: Fig. S2E—H) further indicated that no significant difference in cell cycle was found within the control and the inflammatory groups, ruling out a potential effect of cell proliferation on osteogenic differentiation.

Since inflammation control was a prerequisite for mechanical force application, rats of stable-phase periodontitis were constructed (Fig. 1H). Alveolar bone loss was observed in periodontitis rats by micro CT (Fig. 1I) and hematoxylin and eosin (HE) staining (Additional file 1: Fig. S2I). The tension side of the inflammatory periodontium showed a decrease in trabecular thickness, along with an increase in both trabeculae number and trabecular pattern factor (Fig. 1J). This implied that while the periodontitis periodontium under mechanical force stimulated local bone formation to some extent, the newly remodeled bone showed low density and poor mechanical strength, resulting in an osteoporotic phenotype. Furthermore, the inflammatory group exhibited higher tartrate-resistant acid phosphatase (TRAP) enzyme activity (Fig. 1K, L) and lower ALP protein expression (Fig. 1M, N) after mechanical force application. Consistent with in vitro findings, in vivo data hinted that the inflammatory microenvironment could suppress periodontal bone remodeling driven by mechanical force.

2.2. Inflammatory microenvironment promoted glycolysis and OXPHOS of mechanically stretched periodontal osteoprogenitors

Alterations in cellular metabolic profiles are often associated with their differentiation [32]. The inflammatory mechanical microenvironment exhibited elevated expression of glycolysis-related genes (Fig. 2A, B) and enhanced efflux of lactate, an end product of glycolysis (Fig. 2E). Correspondingly, inflammatory mechanical stimuli promoted phosphorylated PDH-E1α immunofluorescence expression (Fig. 2C, D), implying a more active role of glycolysis in energy production and utilization. More importantly, the following glycolytic parameters in inflammatory groups including glycolysis (Fig. 2G), glycolytic capacity (Fig. 2H), glycolytic reserve (Fig. 2I), and non-glycolytic acidification (Fig. 2J) were increased to varying degrees through extracellular acidification rate (ECAR) detection (Fig. 2F). These demonstrated the inflammatory microenvironment activated the glycolysis of mechanically stretched periodontal osteoprogenitors.

Analogously, OXPHOS also presented positive variations by inflammatory mechanical stimuli. The inflammatory groups exhibited a more enhanced membrane potential (Fig. 3A, B). The active mitochondria within the inflammatory mechanical environment accordingly resulted in an increase in ATP production (Fig. 3C). Although no statistical difference in superoxide anions existed between the control and inflammatory groups (Fig. 3D, E), the NAD^+/NADH ratio was increased by inflammatory mechanical stimuli (Fig. 3F). Additionally, parameters of oxidative metabolism (Fig. 3G), including basal respiration (Fig. 3I), ATP-linked respiration (Fig. 3J), and recovery respiration with FCCP (Fig. 3K), exhibited an ascending response to inflammatory mechanical

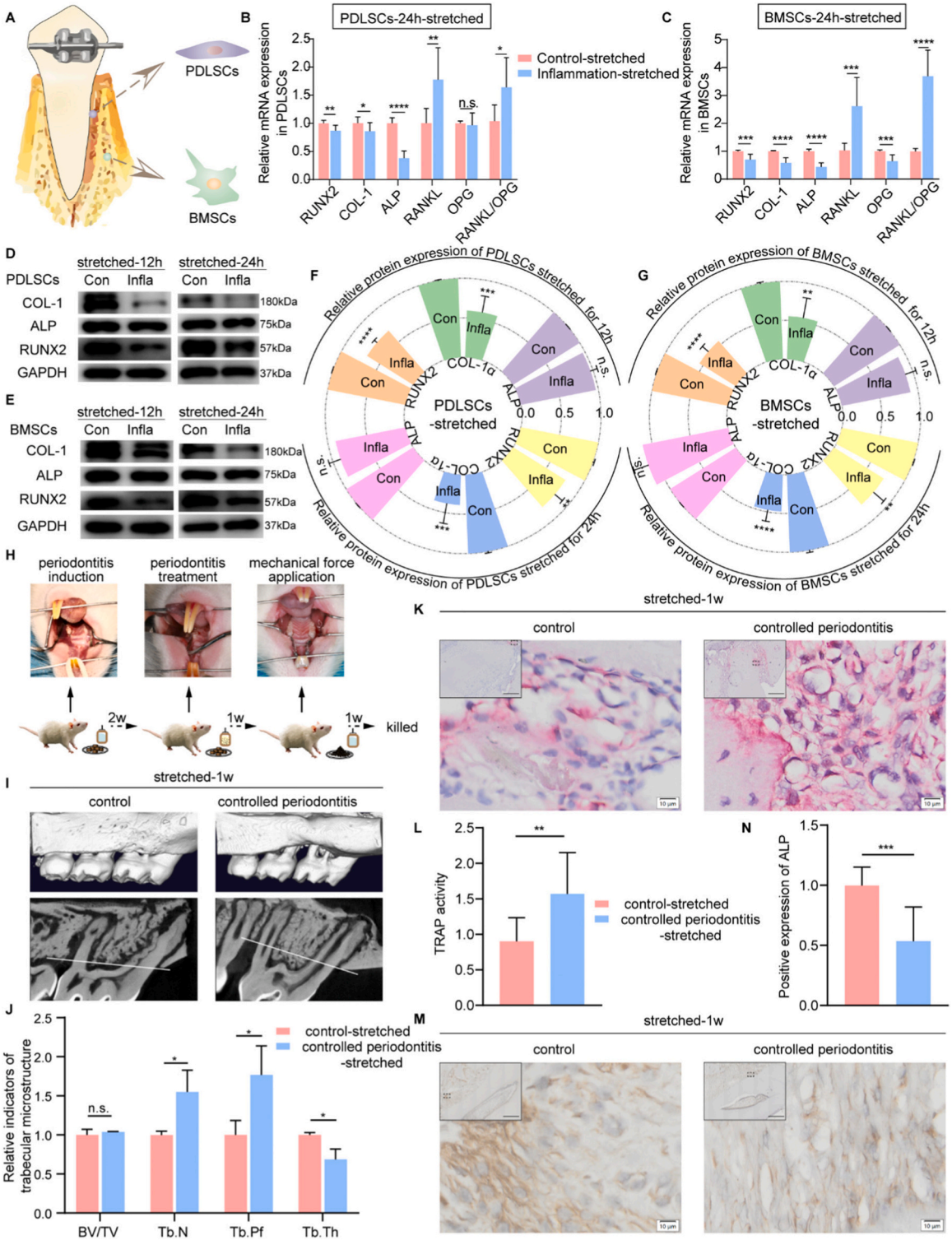

Fig. 1. Inflammatory microenvironment impaired the bone remodeling of periodontium under mechanical force. A. A schematic representation of mechanotransduced cells in periodontium under mechanical force. B—C. mRNA quantification of ALP, RUNX2, COL-1, RANKL, OPG, and RANKL/OPG ratio by qRT-PCR in PDLSCs/BMSCs and iPDLSCs/iBMSCs groups mechanically stimulated for 24 h. $n = 3$. D-G. Protein levels of ALP, RUNX2, and COL-1 by western blot (D, E) and quantification (F, G) by image J in mechanically stimulated PDLSCs/BMSCs and iPDLSCs/iBMSCs groups. $n = 3$. H. Construction of mechanically stimulated models in control/periodontitis rats. I. Representative micro-CT images of mechanically stimulated models in control/periodontitis rats. $n = 3$. The white lines represent alveolar bone height. J. Quantification of BV/TV, Tb.N, Tb.Pf, Tb.Th of mechanically stimulated models in control/periodontitis rats. $n = 3$. K-L. Representative TRAP staining images (K) and quantification analysis (L) of mechanically stimulated models in control/periodontitis rats. $n = 3$. Scale bar, 300 μm (upper panel); Scale bar, 10 μm (lower panel). M-N. Representative ALP immunohistochemical images (M) and quantification analysis (N) of mechanically stimulated models in control/periodontitis rats. $n = 3$. Scale bar, 300 μm (upper panel); Scale bar, 10 μm (lower panel). (*$p < 0.05$; **$p < 0.01$; ***$p < 0.001$; ****$p < 0.0001$; n.s., no significance; Con, control; Infla, Inflammation; BV/TV, bone volume fraction; Tb.N, trabecular number; Tb.Pf, trabecular pattern factor; Tb.Th, trabecular thickness.)

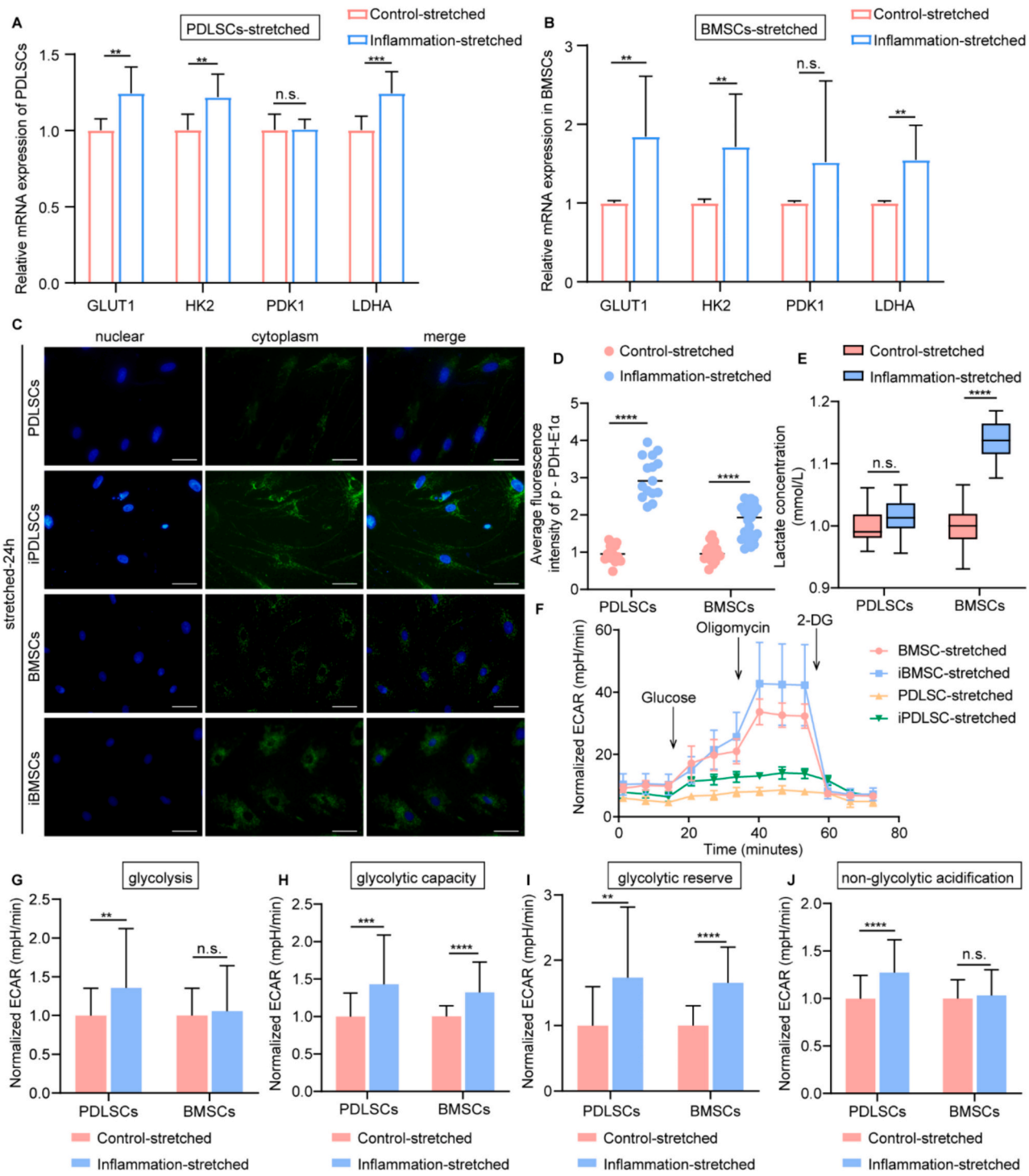

Fig. 2. Inflammatory microenvironment promoted glycolysis of mechanically stretched periodontal osteoprogenitors. A-B. Quantification of GLUT1, HK2, PDK1, and LDHA mRNA by qRT-PCR in mechanically stimulated PDLSCs/BMSCs and iPDLSCs/iBMSCs groups. $n = 3$. C—D. Immunofluorescence image (C) and quantification results (D) of p-PDHE1α in mechanically stimulated PDLSCs/BMSCs and iPDLSCs/iBMSCs groups. $n = 3$. Scale bar, 100 μm. E. The lactate concentration of mechanically stimulated PDLSCs/BMSCs and iPDLSCs/iBMSCs groups. $n = 4$. F-J. Representative ECAR image (F) and quantification analysis of glycolysis (G), glycolytic capacity (H), glycolytic reserve (I), non-glycolytic acidification (J) in mechanically stimulated PDLSCs/BMSCs and iPDLSCs /iBMSCs groups. $n = 3$. (**p < 0.01; ***p < 0.001; ****p < 0.0001; n.s., no significance.)

stimuli. Despite a widespread increase in mitochondrial OXPHOS, proton leak-based results (Fig. 3H) indicated the absence of mitochondrial damage events. Surprisingly, our findings indicated that the inflammatory mechanical microenvironment could result in a simultaneous augmentation of glycolysis and OXPHOS.

2.3. Effects of altered metabolic patterns on mechanically induced bone remodeling during inflammation

The distinct contributions of enhanced glycolysis and OXPHOS in mechanically induced bone remodeling were further explored. GNE-140 has been shown the specificity in targeting LDHA and LDHB to inhibit

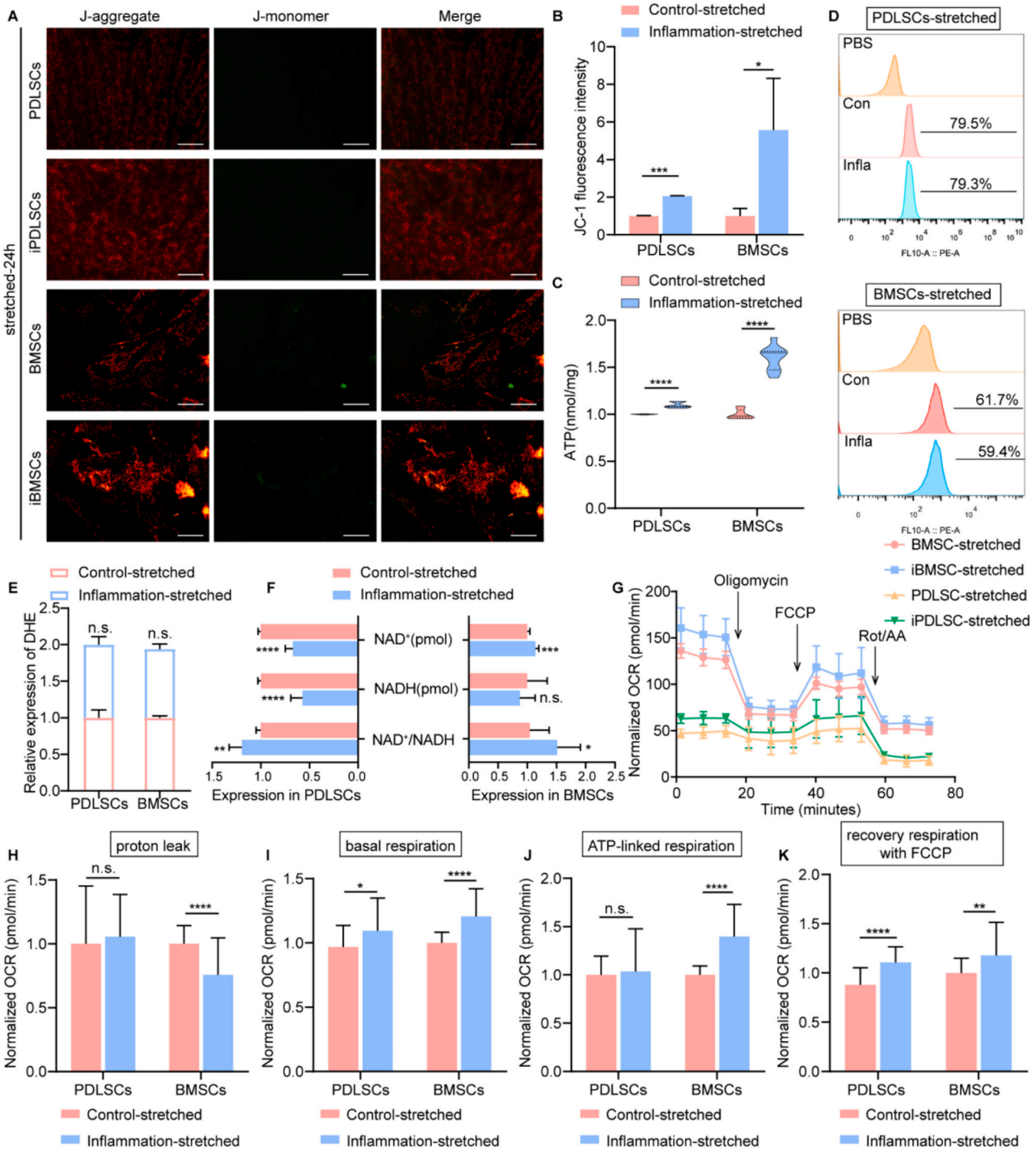

Fig. 3. Inflammatory microenvironment enhanced OXPHOS of mechanically stretched periodontal osteoprogenitors. A-B. The mitochondrial membrane potential level by JC-1 staining (A) and its quantification results (B) by flow cytometry in mechanically stimulated PDLSCs/BMSCs and iPDLSCs/iBMSCs groups. $n = 3$. Scale bar, 100 μm. C. The ATP production of mechanically stimulated PDLSCs/BMSCs and iPDLSCs/iBMSCs groups. n = 3. D-E. Superoxide generation using DHE (D) and its quantification results by flow cytometry (E) in mechanically stimulated PDLSCs/BMSCs and iPDLSCs/iBMSCs groups. n = 3. F. The concentration of NAD^+, NADH, NAD^+/NADH in mechanically stimulated PDLSCs/BMSCs and iPDLSCs/iBMSCs groups. PDLSCs/iPDLSCs groups: n = 3; BMSCs/iBMSCs groups: n = 4. G-K. Representative OCR image (G) and quantification analysis of proton leak (H), basal respiration (I), ATP-linked respiration (J), recovery respiration with FCCP (K) in mechanically stimulated PDLSCs/BMSCs and iPDLSCs/iBMSCs groups. $n = 3$. (*$p < 0.05$; **$p < 0.01$; ***$p < 0.001$; ****$p < 0.0001$; n.s., no significance.)

lactate secretion, consequently impeding fermentative glycolysis [33]. Glycolysis suppression reduced cell proliferation even at low concentrations of GNE-140 (Fig. 4A), which demonstrated the glycolytic necessity in performing basic cellular activities. Based on qRT-PCR and western blots assays, glycolysis inhibition impeded the osteogenic differentiation and promoted osteoclastogenesis of PDLSCs within the inflammatory mechanical microenvironment (Fig. 4B, D, E), indicating the pro-osteogenic role of glycolysis in stretched iPDLSCs. However, glycolysis suppression resulted in a reduction of most osteogenic markers along with a decrease of the osteoclast-promoting factor RANKL in BMSCs within the inflammatory mechanical microenvironment (Fig. 4C-E). Nevertheless, the RANKL/OPG ratio showed a slight upward

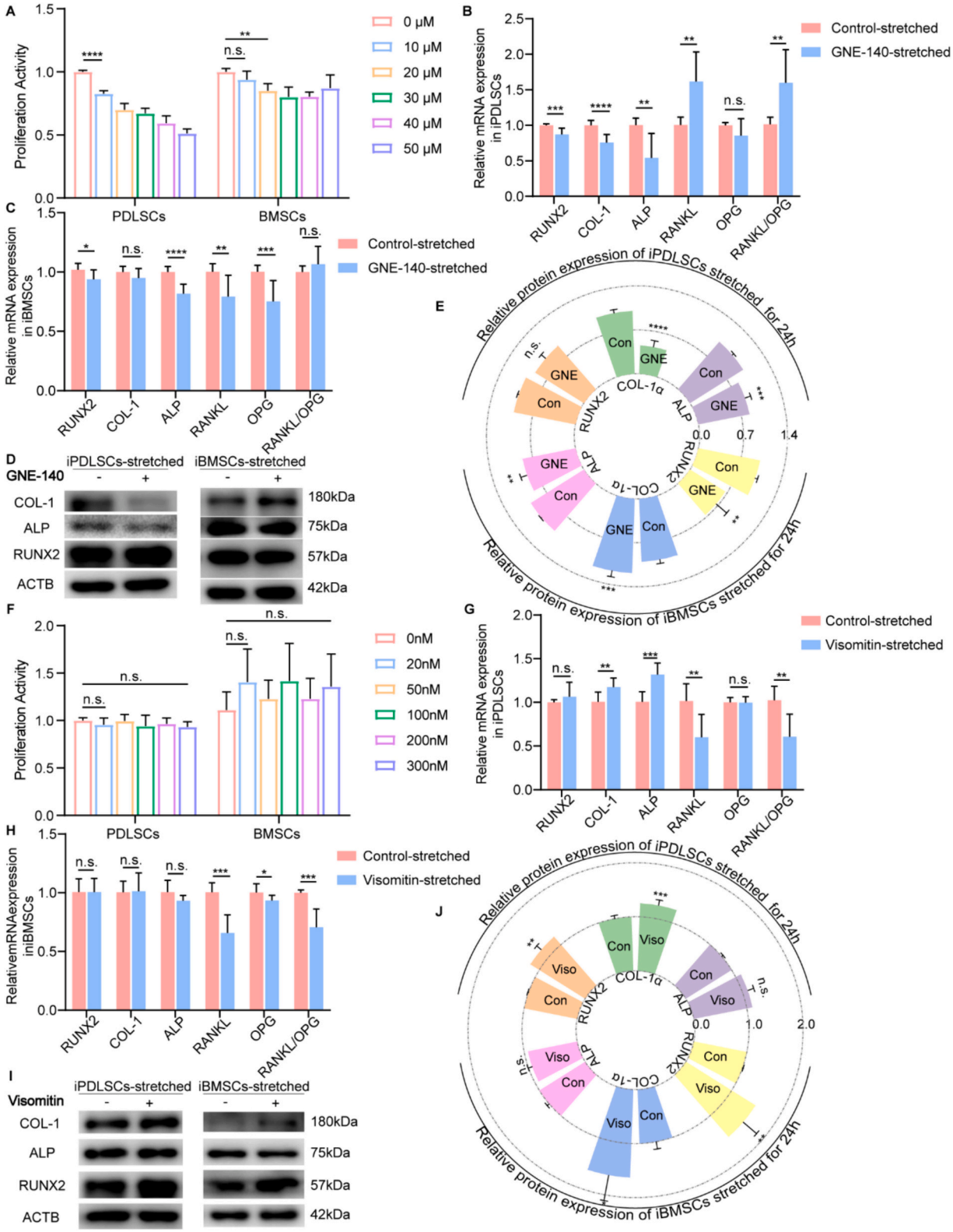

Fig. 4. Effects of altered metabolic patterns on mechanically induced bone remodeling during inflammation. A. Different concentrations of GN*E*-140 on cellular proliferation activity in PDLSCs and BMSCs by CCK-8 assay. $n = 3$. B—C. mRNA quantification of ALP, RUNX2, COL-1, RANKL, OPG, and RANKL/OPG ratio by qRT-PCR in mechanically stimulated iPDLSCs (B) and iBMSCs (C) groups with 10 μM GNE-140 induction. n = 3. D-E. Protein levels of ALP, RUNX2, and COL-1 by western blot (D) and quantification by image J (E) in mechanically stimulated iPDLSCs and iBMSCs groups with 10 μM GNE-140 induction. n = 3. F. Different concentrations of Visomitin on cellular proliferation activity in PDLSCs and BMSCs by CCK-8 assay. n = 3. G-H. mRNA quantification of ALP, RUNX2, COL-1, RANKL, OPG, and RANKL/OPG ratio by qRT-PCR in mechanically stimulated iPDLSCs (G) and iBMSCs (H) groups with 20 nM Visomitin induction. n = 3. I-J. Protein levels of ALP, RUNX2, and COL-1 by western blot (I) and quantification by image J (J) in mechanically stimulated iPDLSCs and iBMSCs groups with 20 nM Visomitin induction. n = 3. (*$p < 0.05$; **$p < 0.01$; ***$p < 0.001$; ****$p < 0.0001$; n.s., no significance; Con, control; GEN, GEN-140; Viso, Visomitin.)

trend due to greater inhibition of OPG expression (Fig. 4C). The diminished pro-osteogenic effects of glycolysis in stretched iBMSCs compared to stretched iPDLSCs might be attributed to the greater reliance of BMSCs on glycolysis for multiple differentiation and functionality.

Visomitin has been demonstrated to inhibit OXPHOS by reducing the OCR of ATP-linked respiration and recovery respiration with FCCP [34]. Additionally, Visomitin was found to suppress the expression of COX4, a pivotal protein regulating the OXPHOS system, at both the transcriptional and translational levels in periodontal osteoprogenitors

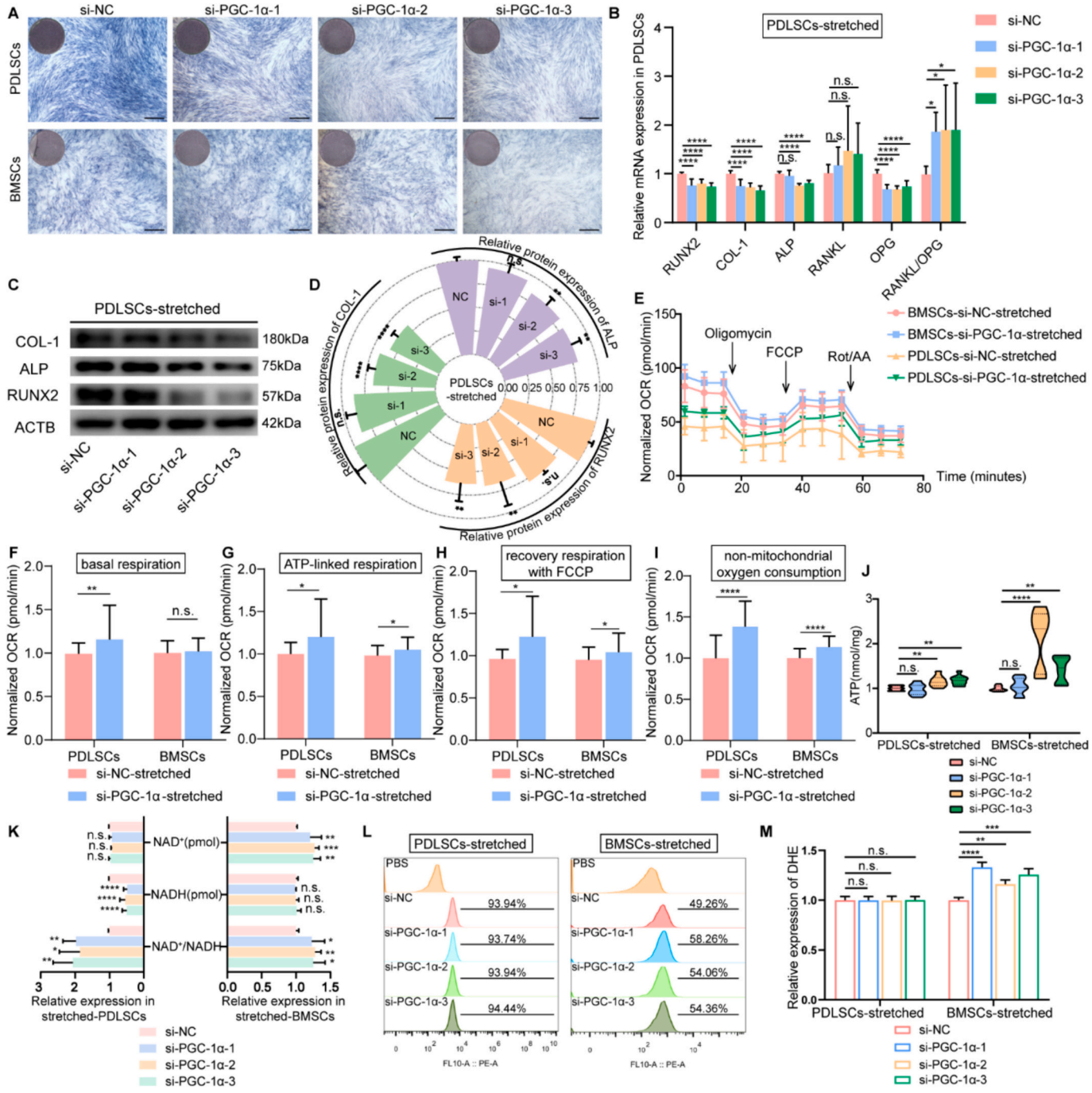

Fig. 5. PGC-1α knockdown enhanced OXPHOS to impede the osteogenic potential of mechanically stretched periodontal osteoprogenitors. A. The ALP staining of PDLSCs and BMSCs with si-NC/si-PGC-1α transfection for 7-day osteogenic induction. n = 3. Scale bar, 500 μm. B. mRNA quantification of ALP, RUNX2, COL-1, RANKL, OPG, and RANKL/OPG ratio by qRT-PCR in mechanically stimulated PDLSCs with si-NC/si-PGC-1α transfection. n = 3. C—D. Protein levels of ALP, RUNX2, and COL-1 by western blot (C) and quantification by image J (D) in mechanically stimulated PDLSCs with si-NC/si-PGC-1α transfection. n = 3. *E*-I. Representative OCR image (E) and quantification analysis of basal respiration (F), ATP-linked respiration (G), recovery respiration with FCCP (H), non-mitochondrial oxygen consumption (I) in mechanically stimulated PDLSCs and BMSCs groups with si-NC/si-PGC-1α transfection. n = 3. J. The ATP production of mechanically stimulated PDLSCs and BMSCs groups with si-NC/si-PGC-1α transfection. n = 3. K. The concentration of NAD^+, NADH, and NAD^+/NADH in mechanically stimulated PDLSCs and BMSCs groups with si-NC/si-PGC-1α transfection. n = 3. L-M. Superoxide generation using DHE (L) and its quantification results by flow cytometry (M) in mechanically stimulated PDLSCs and BMSCs groups with si-NC/si-PGC-1α transfection. n = 3. (*p < 0.05; **p < 0.01; ***p < 0.001; ****p < 0.0001; n.s., no significance; si-1, si-PGC-1α-1; si-2, si-PGC-1α-2; si-3, si-PGC-1α-3.)

(Additional file 1: Fig. S4A—D). Different from the results of glycolysis inhibition, notable disparity in cell viability was absent when OXPHOS was suppressed (Fig. 4F). The administration of the antioxidant Visomitin down-regulated the release of osteoclast-related factors (Fig. 4G, H) and promoted the expression of osteogenesis-related proteins (Fig. 4I, J) accordingly under inflammatory mechanical stimuli.

Based on these observations, we speculated that glycolysis facilitated osteogenic differentiation in mechanically stretched periodontal osteoprogenitors during inflammation, whereas OXPHOS impeded this process.

2.4. Identification and validation of PGC-1α as a key regulator associated with metabolic patterns to regulate the mechanically induced bone remodeling

To investigate the underlying mechanism by which inflammation regulated mechanically stimulated bone remodeling by modulating metabolic patterns, the Reactome database was utilized to predict proteins associated with stress, osteogenesis, and mitochondria. The Venn diagram analysis revealed the intersection of PGC-1α and HDAC3 proteins (Additional file 1: Fig. S3A). Considering the sensitivity of PGC-1α to OXPHOS and its roles in inflammatory diseases [35], we speculated that PGC-1α might modulate mechanically induced bone remodeling through the shift of metabolic patterns.

The findings demonstrated that the expression of PGC-1α exhibited a downward response to inflammatory mechanical stimuli in vitro (Additional file 1: Fig. S3B—F). Consistently, a reduction of PGC-1α expression was also shown in tissue sections from mechanically stimulated rat models with periodontitis (Additional file 1: Fig. S3G, H).

To assess the impact of PGC-1α on bone homeostasis, siRNAs were employed to suppress PGC-1α expression (Additional file 1: Fig. S5A-D). The outcomes of ALP staining demonstrated that PGC-1α reduction exerted no substantial influence on intercellular mineralization during the short-term osteogenic induction mediated by mechanical force (Additional file 1: Fig. S6A). However, it significantly impeded mineralization in PDLSCs and BMSCs following a 7-day exposure to osteogenic induction medium (Fig. 5A). Nevertheless, qRT-PCR and western blot analyses revealed that PGC-1α knockdown decreased the expression of osteogenesis-related markers and increased the production of osteoclastogenic factors even with the short-term stimuli of stretch (Fig. 5B-D; Additional file 1: Fig. S6B—D). These findings suggested that PGC-1α knockdown was unbeneficial to bone formation.

Metabolic indicators were subsequently measured following si-PGC-1α transfection. PGC-1α knockdown elevated oxygen consumption rate (OCR) (Fig. 5E) of basal respiration (Fig. 5F), ATP-linked respiration (Fig. 5G), recovery respiration with FCCP (Fig. 5H), and non-mitochondrial oxygen consumption (Fig. 5I). The total ATP production showed a corresponding increase (Fig. 5J). Furthermore, the suppression of PGC-1α up-regulated the NAD^+/NADH ratio (Fig. 5K) and the intracellular superoxide (Fig. 5L, M). The augmented mitochondrial membrane potential (Additional file 1: Fig. S7A-E) and unaltered proton leak (Additional file 1: Fig. S7F) substantiated the absence of mitochondrial damage, indicating the oxidative stress was independent of mitochondrial dysfunction. Additionally, the glycolysis-related mRNAs exhibited lower expression with si-PGC-1α transfection (Additional file 1: Fig. S8A, B). No significant differences were observed in ECAR of glycolysis, glycolytic capacity, and non-glycolytic acidification between the si-NC and si-PGC-1α groups (Additional file 1: Fig. S8C-E). These demonstrated that PGC-1α knockdown redirected the cellular metabolic profile towards OXPHOS to hinder mechanically induced osteogenesis.

2.5. PGC-1α overexpression promoted glycolysis to rescue inhibited bone remodeling within the inflammatory mechanical microenvironment

We next evaluated whether overexpressed PGC-1α could alleviate the inhibition of bone remodeling within inflammatory mechanical microenvironment by metabolic regulation. The overexpression efficacy of PGC-1α was confirmed via qRT-PCR and western blot assays (Additional file 1: Fig. S9A-E). Compared to the ov-NC groups, ov-PGC-1α transfection markedly reversed the osteogenic markers expression and decreased the osteoclast promoting of inflammatory periodontal osteoprogenitors with 24-h mechanical stimulation (Fig. 6A-F). Although stretched ov-PGC-1α groups did not result in any significant changes in either ALP protein levels (Fig. 6C-F) or ALP activity (Additional file 1: Fig. S10A, B), the mineralization of inflammatory PDLSCs (iPDLSCs), as assessed by ALP staining, showed a noteworthy enhancement following a 7-day induction with osteogenic medium (Fig. 6G). Interestingly, the mineralization of induced iBMSCs displayed no significant alteration (Additional file 1: Fig. S10C), potentially attributable to the inherent variability in cellular responses to osteogenic indicators among different cell species.

Consistent with our initial hypothesis, PGC-1α overexpression led to an increase in the expression of glycolysis-related genes during inflammation (Fig. 6H, I), as well as an elevation in ECAR (Fig. 6J) pertaining to glycolysis (Fig. 6K), glycolytic capacity (Fig. 6L) and glycolytic reserve (Fig. 6M). Intriguingly, the onset of glycolysis did not result in an extracellular acidic microenvironment (Additional file 1: Fig. S11I; Fig. 7G). Additionally, a general decrease or meaningless change of OCR values (Additional file 1: Fig. S11C —H) was detected in the ov-PGC-1α groups. Correspondingly, ov-PGC-1α transfection resulted in a decrease in total ATP production (Fig. 6N), as well as a suppression of oxidative stress indicators such as the NAD^+/NADH ratio (Fig. 6O) and the intracellular superoxide (Fig. 6P, Q). Notably, PGC-1α overexpression also corresponded to an augmentation in mitochondrial membrane potential (Additional file 1: Fig. S11A, B) without any concurrent increase in proton leak (Additional file 1: Fig. S11D), ruling out the possibility that the altered metabolic pathway was caused by mitochondrial dysfunction.

These implied that the restoration of impaired osteogenic potential due to inflammatory mechanical signals through PGC-1α overexpression was associated with an augmentation of glycolysis rather than OXPHOS.

2.6. PGC-1α regulated the glycolysis by modulating the transcription, translation, and metabolite levels of LDHA

LDHA played a crucial role in glycolysis by altering the metabolic pathway of pyruvate, a commonly found substrate in both glycolysis and OXPHOS [28]. Therefore, we investigated whether the promotion of glycolysis through PGC-1α overexpression was mediated by the interaction between LDHA and PGC-1α. The mRNA levels of LDHA displayed the same variation tendency as PGC-1α (Additional file 1: Fig. S8A, B; Fig. 6H, I). Nevertheless, PGC-1α overexpression had no effects on LDHA promoter activity (Fig. 7A), suggesting the indirectness of transcription modulation. The protein levels of LDHA also exhibited a similar pattern of variation as that of PGC-1α (Fig. 7B-E).

Considering the potential counterproductive effects of lactate accumulation produced by LDHA, we further examined the impact of suppressed and overexpressed PGC-1α on lactate levels. The si-2 and si-3 sequences were selected for their more pronounced effects on bone remodeling when evaluating the influence of PGC-1α knockdown. The data showed that the shift towards OXPHOS due to PGC-1α inhibition did not alter the extracellular lactate level (Fig. 7F). Surprisingly, the occurrence of glycolysis caused by PGC-1α overexpression resulted in a decrease in lactate efflux (Fig. 7G) and an elevation in LDH activity (Fig. 7H), without the unfavorable acidification caused by lactate accumulation. These implicated PGC-1α could regulate LDHA through multiple mechanisms, including transcription, translation, and metabolite activities.

However, the way that PGC-1α regulated LDHA in a content-dependent manner could not explain the glycolysis promotion in the inflammatory mechanical environment. Interestingly, protein-protein docking analysis (Fig. 7I) and co-immunoprecipitation assays (Fig. 7J)

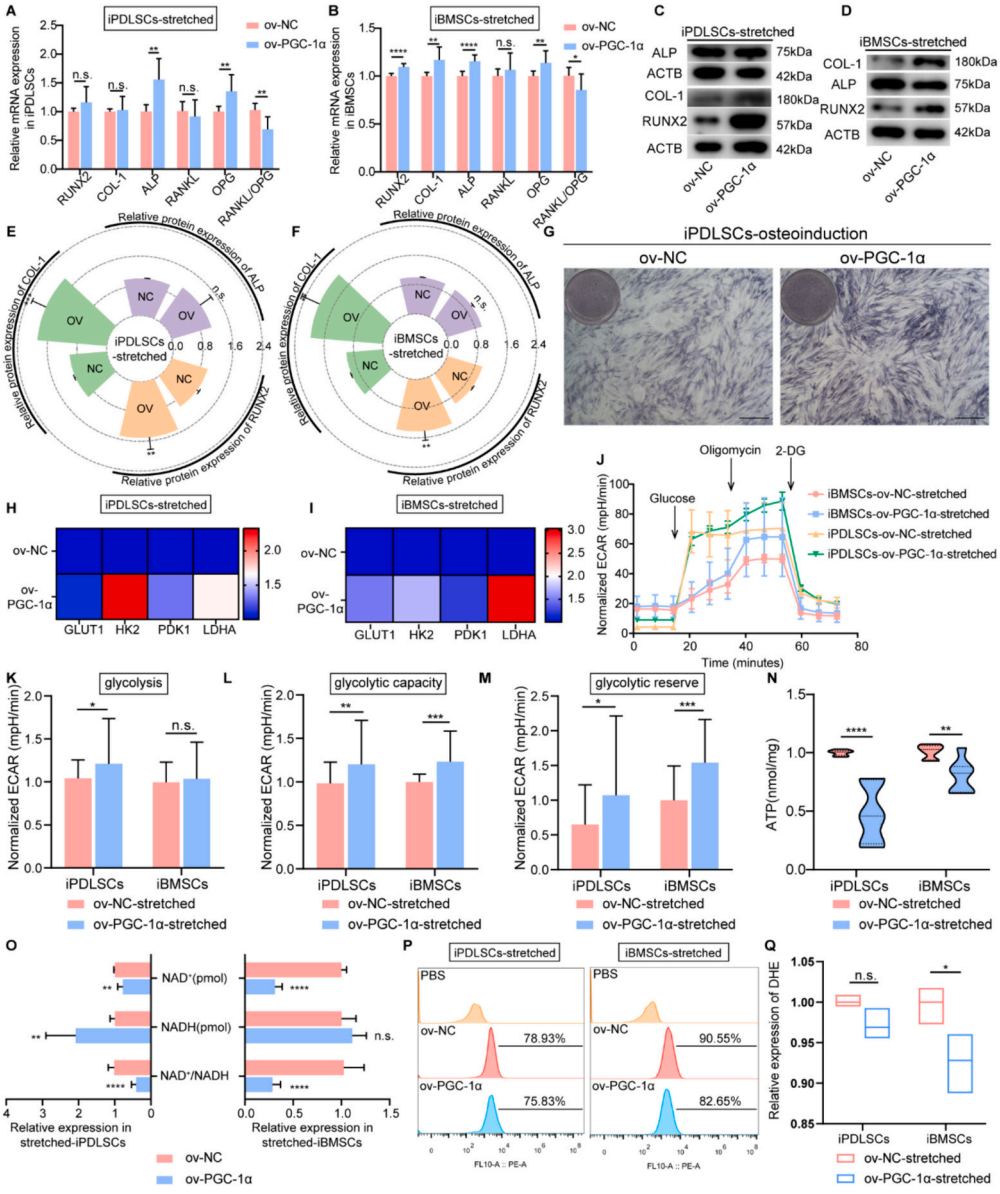

Fig. 6. PGC-1α overexpression promoted glycolysis to rescue inhibited bone remodeling within inflammatory mechanical microenvironment. A-B. mRNA quantification of ALP, RUNX2, COL-1, RANKL, OPG, and RANKL/OPG ratio by qRT-PCR in mechanically stimulated iPDLSCs (A) and iBMSCs (B) groups with ov-NC/ov-PGC-1α transfection. n = 3. C—F. Protein levels of ALP, RUNX2, and COL-1 by western blot (C, D) and quantification by image J (E, F) in mechanically stimulated iPDLSCs/iBMSCs groups with ov-NC/ov-PGC-1α transfection. n = 3. G. The ALP staining of iPDLSCs with ov-NC/ov-PGC-1α transfection for 7-day osteogenic induction. n = 3. Scale bar, 500 μm. H—I. Heatmap of GLUT1, HK2, PDK1, and LDHA mRNA by qRT-PCR in mechanically stimulated iPDLSCs (H) and iBMSCs (I) groups with ov-NC/ov-PGC-1α transfection. n = 3. J-M. Representative ECAR image (J) and quantification analysis of glycolysis (K), glycolytic capacity (L), and glycolytic reserve (M) in mechanically stimulated iPDLSCs and iBMSCs groups with ov-NC/ov-PGC-1α transfection. n = 3. N. The ATP production of mechanically stimulated iPDLSCs and iBMSCs groups with ov-NC/ov-PGC-1α transfection. n = 3. O. The concentration of NAD^+, NADH, and NAD^+/NADH in mechanically stimulated iPDLSCs and iBMSCs groups with ov-NC/ov-PGC-1α transfection. n = 3. P-Q. Superoxide generation using DHE (P) and its quantification results by flow cytometry (Q) in mechanically stimulated iPDLSCs and iBMSCs groups with ov-NC/ov-PGC-1α transfection. n = 3. (*p < 0.05; **p < 0.01; ***p < 0.001; ****p < 0.0001; n.s., no significance.)

revealed a stable binding between PGC-1α (purple) and LDHA (blue). This binding was found to be enhanced by inflammatory mechanical stimuli (Fig. 7K, L), which might stabilize and activate LDHA [36–38], thereby facilitating osteoprotective glycolysis to some extent.

2.7. LDHA inhibition largely eliminated the bone repair effect of overexpressed PGC-1α within the inflammatory mechanical microenvironment

To demonstrate that the interaction of PGC-1α with LDHA was involved in bone remodeling, LDHA was suppressed (Additional file 1: Fig. S12A-D) while PGC-1α was overexpressed simultaneously during inflammation. Osteogenic markers of stretched iPDLSCs in the ov-PGC-1α + si-LDHA group were downregulated compared to those in the ov-PGC-1α + si-NC group (Fig. 8A, C, E, G). In addition, si-LDHA inhibition increased the RANKL/OPG ratio through lower levels of OPG, but unaffected levels of RANKL (Fig. 8C). Similarly, in PGC-1α-overexpressed stretched iBMSCs, although LDHA knockdown did not significantly impact ALP enzymatic activity (Fig. 8B) and ALP mRNA level (Fig. 8D), it suppressed the protein level of ALP, as well as the gene and protein levels of RUNX2 and COL-1 (Fig. 8D, F, H). Additionally, while LDHA knockdown inhibited RANKL expression in PGC-1α-overexpressed

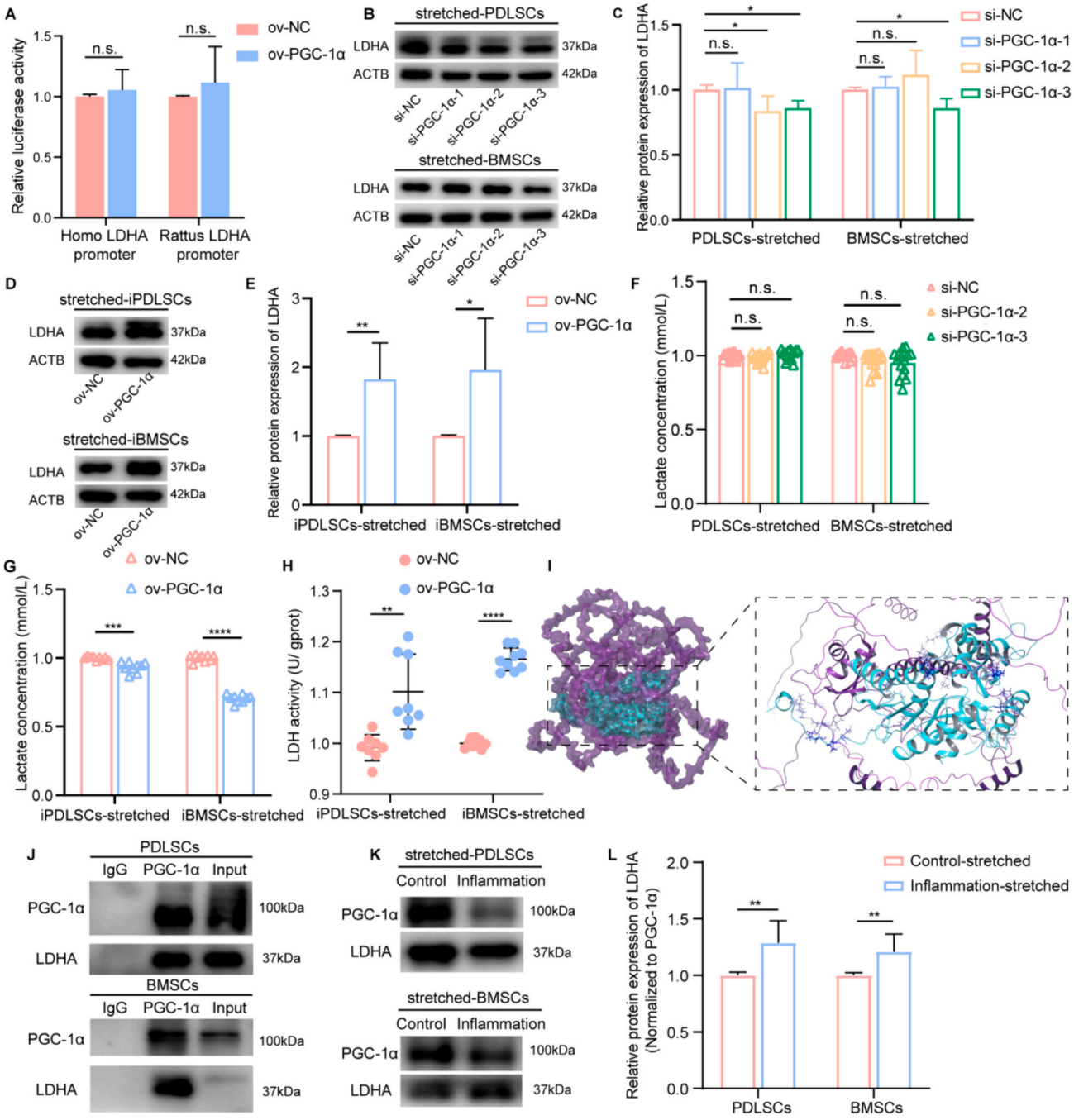

Fig. 7. PGC-1α regulated the glycolysis by modulating the transcription, translation, and metabolite levels of LDHA. A. Luciferase assays for Homo/Rattus LDHA promoter activity with ov-NC/ov-PGC-1α transfection. n = 3. B—C. LDHA protein level by western blot (B) and quantification by image J (C) in mechanically stimulated PDLSCs and BMSCs groups with si-NC/si-PGC-1α transfection. n = 3. D-E. LDHA protein level by western blot (D) and quantification by image J (E) in mechanically stimulated iPDLSCs and iBMSCs groups with ov-NC/ov-PGC-1α transfection. n = 3. F. The lactate concentration of mechanically stimulated PDLSCs and BMSCs groups with si-NC/si-PGC-1α transfection. n = 4. G. The lactate concentration of mechanically stimulated iPDLSCs and iBMSCs groups with ov-NC/ov-PGC-1α transfection. n = 3. H. Quantification of LDH activity in mechanically stimulated iPDLSCs and iBMSCs groups with ov-NC/ov-PGC-1α transfection. n = 3. I. Protein-protein docking analysis of binding sites between PGC-1α (purple) and LDHA (blue). J. Co-immunoprecipitation of PGC-1α with LDHA in PDLSCs and BMSCs. n = 3. K. Co-immunoprecipitation of PGC-1α with LDHA in mechanically stimulated iPDLSCs and iBMSCs. n = 3. L The relative protein quantification of LDHA bound to PGC-1α by image J in mechanically stimulated iPDLSCs and iBMSCs. n = 3. (*p < 0.05; **p < 0.01; ***p < 0.001; ****p < 0.0001; n.s., no significance.) (For interpretation of the references to color in this figure legend, the reader is referred to the web version of this article.)

stretched iBMSCs, the RANKL/OPG ratio showed a slight upward trend due to greater inhibition of OPG expression (Fig. 8D). Despite the cellular variability in osteogenic marker performance, the positive effect of LDHA on osteogenesis was well established.

In light of this, our findings suggested that LDHA knockdown inhibited osteogenesis and largely promoted osteoclastogenesis of periodontal osteoprogenitors overexpressing PGC-1α within the inflammatory mechanical microenvironment. Hence, LDHA inhibition largely eliminated the "bone repair" effect of PGC-1a overexpression within the inflammatory mechanical microenvironment.

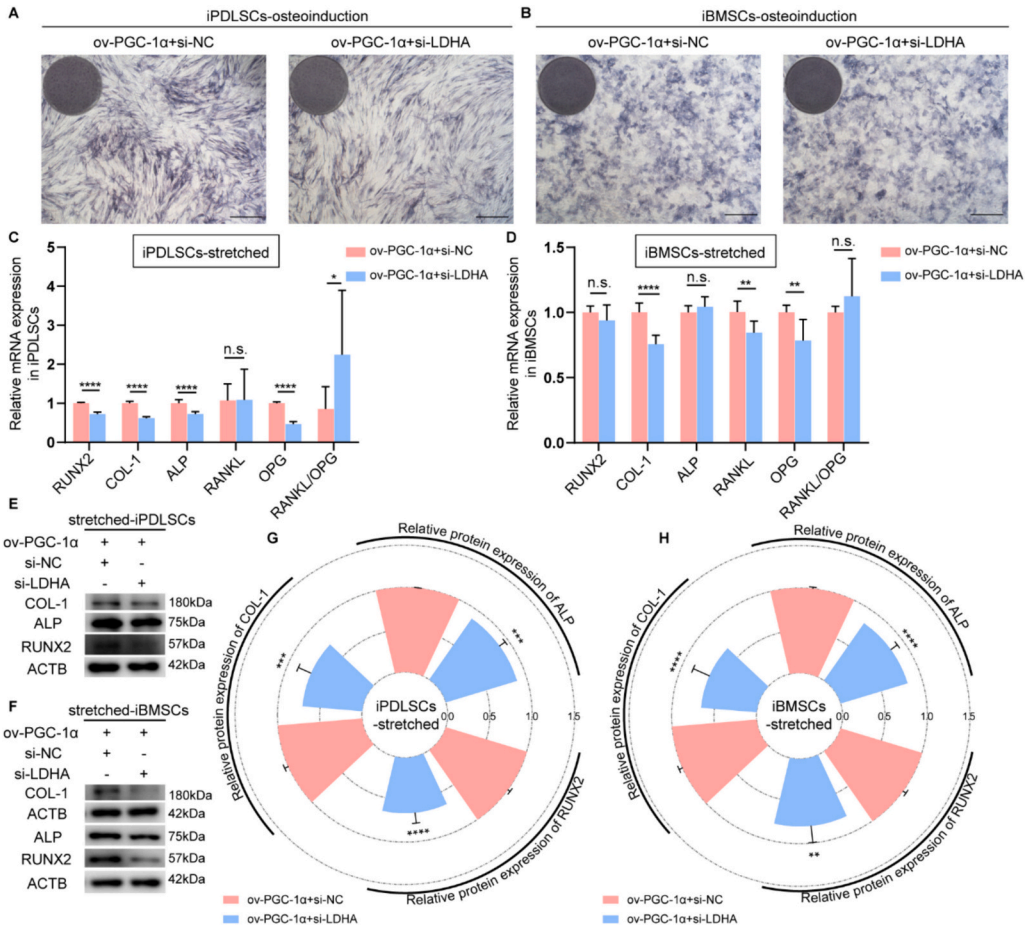

Fig. 8. LDHA inhibition largely eliminated the bone repair effect of overexpressed PGC-1α within the inflammatory mechanical microenvironment. A. The ALP staining of iPDLSCs based on rescue test for 7-day osteogenic induction. n = 3. Scale bar, 500 μm. B. The ALP staining of iBMSCs based on rescue test for 7-day osteogenic induction. n = 3. Scale bar, 500 μm. C—D. mRNA quantification of ALP, RUNX2, COL-1, RANKL, OPG, and RANKL/OPG ratio by qRT-PCR in mechanically stimulated iPDLSCs (C) and iBMSCs (D) groups based on rescue test. n = 3. E-H. Protein levels of ALP, RUNX2, and COL-1 by western blot (E, F) and quantification by image J (G, H) in mechanically stimulated iPDLSCs/iBMSCs groups based on rescue test. iPDLSCs groups: n = 3; iBMSCs groups: $n = 5$. (*p < 0.05; **p < 0.01; ***p < 0.001; ****p < 0.0001; n.s., no significance.)

3. Discussion

Cells and their microenvironments are in a dynamic state of mechanical reciprocity [39]. Thus, tissue remodeling in the inflammatory microenvironment is stimulated by both chemical and mechanical factors. Nevertheless, such mechanical dynamics have rarely been considered. As a key feature of cellular response to inflammatory mechanical stimuli [14], metabolic reprogramming confers a higher energy state to the cells and participates in tissue remodeling by immune cells and stem cells [22,40]. The study of the rationale of metabolic reprogramming in the inflammatory mechanical microenvironment is beneficial for the development of effective drugs to promote tissue reconstruction. Therefore, this work focuses on the glucose metabolic fluxes alterations and their bone remodeling effects in periodontitis under mechanical force. Based on this foundation, the target molecules impacting bone remodeling through orchestrating glycolysis and OXPHOS are further identified and explored. Collectively, this study holds substantial implications for the comprehension of tissue remodeling by metabolic mechanisms in inflammatory diseases within mechanical environments.

According to the findings of our investigations, the inflammatory microenvironment compromised the mechanically induced osteogenesis of periodontal osteoprogenitors, with the release of osteoclast-related active factors. Interestingly, the changes in ALP protein and activity (Additional file 1: Fig. S2C, D) were comparatively less prominent. Although ALP is an early osteogenic differentiation marker secreted by stem cells [41], its protein activity is predominantly observed on day 3 or day 7 [42,43]. However, the material specificity of the Flexcell amino silicone-bottomed plates limits the duration of force application. Hence, insignificant changes in ALP protein in vitro may be due to the insufficient duration of 24-h mechanical stimulation to induce its expression. Additionally, different from previous studies [44,45], cell proliferation showed no response to inflammatory mechanical stimuli, suggesting that mechanical force intervention might influence the outcome of the inflammatory response. The findings in vivo revealed a heightened osteoporotic characteristic in mechanically stimulated rats during the stable periods of periodontitis, consistent with the results in vitro. Notably, the formation of collagen fibers (Additional file 1: Fig. S2J) and the bone volume fraction (Fig. 1J) were not significantly compromised by inflammatory mechanical stimuli. This implies the necessity of periodontitis treatment prior to mechanical force application, which may partially reduce the inflammation-induced bone loss during the active phase [46]. For inflammatory diseases similarly within mechanical environments, this also suggests that inflammation control is a prerequisite for tissue regeneration applications.

The process of bone remodeling in response to mechanical force necessitates a substantial expenditure of energy, which is provided by the primary energy supply pathways of glycolysis [28] and OXPHOS [47]. Thus, we posited that changes in osteogenic potential in stretched periodontal osteoprogenitors were associated with altered metabolic patterns. Intriguingly, we found that the inflammatory mechanical

stimuli elicited a dual enhancement of both metabolic modes. This observation prompted us to contemplate whether these two metabolic modes acted antagonistically or synergistically in mechanically stimulated bone remodeling. Following the administration of inhibitors to regulate metabolic pathways, our findings indicated that glycolysis exhibited a greater propensity towards promoting osteogenesis, whereas OXPHOS showed a somewhat adverse effect on osteogenesis. This implied that the heightened OXPHOS during inflammation led to the inhibition of mechanically stimulated bone remodeling, while the augmented glycolysis during inflammation might represent an adaptive response to evade the potential harms of OXPHOS. Similarly, glycolysis functioned as a metabolic adaptation to enhance the resistance of vascular smooth muscle cells to oxidative stress [48]. However, the adaptive upregulation of glycolysis in cancer cells primarily served the purpose of synthesizing precursors necessary for their rapid proliferation [49]. Interestingly, compared to the pro-osteogenic effects of glycolysis in the non-inflammatory mechanical environment [28], the bone-promoting function of glycolysis does exist but seems to be diminished in the inflammatory mechanical environment. This implies that the metabolic modes and mechanisms in the inflammatory mechanical microenvironment are different from those in the non-inflammatory mechanical microenvironment. In addition, the down-regulation of RANKL in iBMSCs after glycolysis inhibition not only suggests that osteoclastic differentiation of iBMSCs is more dependent on glycolysis, but also may indicate an intermediate state of glycolysis, which initiates a transition from a protective to a destructive impact. These suggest that the metabolic shift of early glycolysis could be advantageous for osteogenesis. However, when lactate accumulated beyond a certain threshold, the acidic microenvironment of late glycolysis might be counterproductive to bone remodeling [50].

OXPHOS occurs within the mitochondria. PGC-1α, a molecule responsible for mitochondrial biogenesis and highly sensitive to OXPHOS [51], plays a crucial role not only in the regeneration of tissues such as vasculature [52], muscle [53], and nerves [54] by modulating cellular metabolism, but also in the pathogenesis of various inflammatory metabolic disorders, including neuritis [55], nephritis [56], and osteoarthritis [57]. These observations combined with database screening results have motivated us to conduct a mechanistic investigation on the role of PGC-1α in the inflammatory mechanical environment. Our findings revealed that PGC-1α knockdown impeded mechanically stimulated osteogenesis through augmented OXPHOS. Conversely, PGC-1α overexpression rescued the impaired osteogenic potential within inflammatory mechanical environments by enhanced glycolysis. While the osteogenic role of PGC-1α aligned with previous studies [57,58], the promotion of glycolysis by PGC-1α differed from the majority of literature, which suggested that up-regulated PGC-1α facilitated OXPHOS [51,59]. This discrepancy might stem from the specificity of the complex microenvironment composed of inflammation and mechanical force. Therefore, we hypothesized that PGC-1α might modulate the rate-limiting enzyme LDHA, which promoted the initiation of glycolysis. Despite the predominant nuclear localization of PGC-1α, it was plausible that post-translational modifications might influence the cellular distribution of PGC-1α [60], thereby facilitating its interaction with LDHA. Significantly, we demonstrated that the overexpression of PGC-1α led to an enhancement of LDHA in glycolysis but a reduction in lactate production. This raises a possibility that cells might possess the capacity for metabolic waste disposal during the early stages of glycolysis, potentially associated with lactate shuttling [61]. This phenomenon also explains why mitochondrial membrane potential and LDH activity are heightened in PGC-1α overexpressed cells, where glycolysis dominates and OXPHOS exits. The regulation of PGC-1α on LDHA in a content-dependent manner explains the enhanced OXPHOS induced by the decreased PGC-1α in the inflammatory mechanical environment. In addition, the increased binding between PGC-1α and LDHA in this environment might also enhance glycolysis in a protein-activated manner to resist OXPHOS effects to some extent. Nevertheless, the upregulation of LDHA mRNA and elevated lactate levels indicates the presence of additional factors influencing glycolysis in this environment, which deserves further investigation.

Despite recent advancements in metabolic research, the utilization of metabolic treatment in chronic inflammatory diseases within mechanical environments remains nascent, primarily due to the heterogeneity of cellular metabolic reactions to inflammatory ailments. Our findings demonstrated the osteogenic functions of metabolic patterns and the mechanism of metabolic regulation based on PGC-1α-LDHA interactions in periodontal osteoprogenitors with inflammatory mechanical stimuli. However, it should be noted that periodontal osteoprogenitors in bone remodeling are not isolated entities, as a reciprocal communication exists between PDLSCs and BMSCs [62]. The current investigation primarily examines their individual response to inflammatory mechanotransduction, and the forthcoming research will concentrate on elucidating the interplay between the two.

4. Conclusions

Altogether, we demonstrate a previously unexplored link between metabolic patterns and their bone remodeling functions in periodontal osteoprogenitors with inflammatory mechanical stimuli. Our observation that PGC-1α-LDHA interaction promotes glycolysis to alleviate the inhibition of bone remodeling within inflammatory mechanical microenvironments provides insights into the molecular mechanisms that integrate metabolism with gene regulation to dictate cell differentiation. This may present a novel metabolic therapeutic strategy for guiding tissue remodeling in inflammatory diseases within mechanical environments.

5. Materials and methods

5.1. Isolation and identification of cells

All experiments involving periodontal tissues in this study were approved by the Medical Ethical Committee of School of Stomatology, Shandong University (No. 20210140). All donors (13 donors; aged 13–20 years; without systemic disease, caries, or periodontitis) or their guardians signed an informed consent form with the content that the teeth were extracted for research purposes. All experiments involving animal tissues in this study were also ethically validated (No. 20200709) by the Committee on the Ethics of Animal Experiments of Shandong University. PDLSCs and BMSCs were isolated and cultivated as previously reported [28,63]. Briefly, the PDL tissue was scraped from the middle third of the root surface and seeded into flasks. The mandibular tissues from ten 4-week-old rats (male) were dissected and treated with collagenase I (3 mg/ml, Solarbio, Beijing, China) and dispase II (4 mg/ml, Roche, Shanghai, China) at 37 °C for 1 h. The tissue pieces were then incubated in α-MEM containing 20 % fetal bovine serum until the primary cells migrated from PDL and mandibular tissue pieces. PDLSCs and BMSCs at passages 2–5 were employed in the subsequent studies. Their stemness was confirmed by flow cytometric analysis and multiple differentiation potential as previously described [63].

5.2. Cell pretreatment

Mechanical force was applied to promote osteoblast differentiation. PDLSCs and BMSCs were seeded on Flexcell amino silicone-bottomed plates at 2×10^5 cells/well. Since gentler mechanical force was preferred in periodontitis patients, a mechanical stimulation with 8 % elongation, 0.1 Hz for 12–24 h was performed by Flexcell® FX-5000TM Tension System (Flexcell International Corp., Burlington, USA) to establish osteogenic conditions when cell density reached 90 % [7]. Cells cultured with α-MEM medium containing 10 % fetal bovine serum served as the control group, while cells cultured with medium supplemented with 10 ng/ml TNF-α (Peprotech, Shanghai, China) were set as

the inflammatory group. When the osteogenic response was insensitive to the mechanical stimulation, cultivate cells with osteogenic induction medium supplemented with 50 μg/ml vitamin C (Sigma-Aldrich, St. Louis, USA), 10 mM β-glycerophosphate disodium salt hydrate (Sigma-Aldrich, St. Louis, USA), and 0.1 μM dexamethasone (Sigma-Aldrich, St. Louis, USA). To inhibit cellular glycolysis, cells were pretreated with GNE-140 [33] (10 μM, MedChemExpress, Shanghai, China) for 12 h. To suppress cellular oxidation, cells were preincubated with Visomitin [34] (20 nM, MedChemExpress, Shanghai, China) for 2 h. Subsequently, mechanical loading was carried out to observe the effects of different metabolic modes on cellular osteogenic capacity.

5.3. Cell transfection

PDLSCs and BMSCs were plated at an initial density of 2×10^5 cells per well. When cell confluence reached 70 %–80 %, the following treatments were performed.

5.3.1. si-RNA transfection

The si-NC or si-PGC-1α/si-LDHA (Hanheng Biology, Shanghai, China) was diluted to 50 nM with opti-MEM (Gibco, CA, USA) and mixed with lip2000 (Thermo Fisher Scientific, Massachusetts, USA) working solution. After standing for 20 min, the mixture of siRNA-lipo2000 complex was added to cells and incubated at 37 °C and 5 % CO_2 for 1 h. Subsequently, cells were cultured under mechanical force for 24 h. The sequences of siRNAs were listed in Additional file 4: Supplementary Table 1.

5.3.2. Lentiviral transfection

Half-volume infection was utilized as a method to complete transfection. Cells were infected with ov-NC or ov-PGC-1α (Hanheng Biology, Shanghai, China) at 3 multiplicity of infection with the assistance of polybrene (4μg/ml). After 4 h of infection with a half-volume mixture, the medium was replenished to the full culture volume. The culture medium was then replaced with a virus-free culture medium after 24-h transfection. The plates were incubated at 37 °C for another 24 h. The medium was supplemented with 10 ng/ml TNF-α prior to the application of mechanical stimuli.

5.4. qRT-PCR

Total RNAs were extracted from samples firstly. 1μg of RNA was reverse transcribed using the Evo M-MLV RT Kit (Accurate Biology, Changsha, China). The generated cDNA was amplified and analyzed through qRT-PCR system (LightCycler® 96 SW 1.1, Roche Ltd., Switzerland) using the SYBR® Green Premix Pro Taq HS qPCR Kit (Accurate Biology, Changsha, China). Reactions were performed in triplicate and normalized to β-actin or GAPDH as indicated. The primer sequences for qRT-PCR were shown in Additional file 4: Supplementary Table 2.

5.5. Western blots

Samples were first subjected to protein extraction, lysis, and denaturation. The denatured proteins were subsequently electrophoresed, transferred, and incubated overnight with the following antibodies depending on different experimental purposes: anti-GAPDH (1:10000, 10494–1-AP, Proteintech, Wuhan, China), anti-ACTB (1:10000, 20536–1-AP, Proteintech, Wuhan, China), anti-RUNX2 (1:500, SD208–0, Huaan Biotechnology), anti-ALP (1:500, SA40–00, HuaBio, Hangzhou, China), anti-COL-1 (1:1000, 14695–1-AP, Proteintech, Wuhan, China), anti-LDHA (1:1000, ab52488, Abcam, MA, USA; 1:1000, 19987–1-AP, Proteintech, Wuhan, China), anti-PGC-1α (1:1000, 66369–1-lg, Proteintech, Wuhan, China), anti-COX4 (1:1000, 11242–1-AP, Proteintech, Wuhan, China). The gray value of the blots was calculated by Image J (NIH, Bethesda, USA) to quantify protein expression.

5.6. ALP staining

Following PBS rinses, the cells were fixed with 4 % paraformaldehyde for 20 min. After washing again, ALP staining was performed according to the protocol of BCIP/NBT Alkaline Phosphatase Color Development Kits (Sigma-Aldrich, St. Louis, USA; Beyotime, Shanghai, China).

5.7. Cell counting kit-8 (CCK-8) assay

Cell proliferation activity was evaluated by CCK-8 assay kits (Biosharp Life Sciences, Anhui, China). Briefly, the CCK-8 solution was mixed with α-MEM containing 10 % fetal bovine serum at a ratio of 1:10. Subsequently, the initial medium was removed and the cells were incubated with the mixture for 1 h at 37 °C with 5 % CO_2. The Absorbance was measured and analyzed at 450 nm.

5.8. Cell cycle assessment

Trypsin-digested cells were washed once with PBS and immediately resuspended and fixed with 70 % prechilled ethanol overnight at 4 °C. The stoichiometric binding of propidium iodide to intracellular DNA was assessed using DNA Content Quantitation Assay (Cell Cycle) Kits (Solarbio, Beijing, China) and quantified by flow cytometry.

5.9. Immunofluorescence

Following the 20-min fixation with 4 % paraformaldehyde, cells were permeated by 0.1 % Triton X-100 for 5 min and blocked with goat serum for 30 min. The samples were subsequently incubated overnight at 4 °C with the following antibodies: anti-p-PDH-E1α (1:400, #37115S, Cell Signaling Technology, MA, USA), anti-PGC-1α (1:200, 66369–1-lg, Proteintech, Wuhan, China). The next day, the rinsed samples were hybridized with secondary antibodies conjugated with fluorochrome for 1 h at room temperature and protected from light. Afterwards, the nucleus was counterstained by DAPI staining. Cellular images were visualized through the Leica DMi8 microsystems (Lecia, Wetzlar, Germany). Notably, due to the special configuration of the amino silicone-bottomed plates, the maximum magnification of fluorescent images was limited to 20×.

5.10. Lactate assay

The supernatant was collected and reacted sequentially with enzyme working solution and chromogen solution according to instructions of the lactic acid assay kit (Nanjing Jiancheng Bioengineering Institute, Nanjing, China). The mixture was incubated at 37 °C for 10 min. After the reaction was terminated, absorbance representing extracellular lactate levels was measured at 530 nm optical density.

5.11. Intracellular ATP content assay

ATP levels were determined by the ATP assay kit (Beyotime, Shanghai, China). Briefly, cells were lysed using the ATP detection lysate. After centrifugation and aspiration of the supernatant, the ATP detection working solution was added. The luminescence based on ATP levels was detected by a luminometer. The calculated ATP concentration was homogenized by the protein concentration of the ATP supernatant.

5.12. NAD^+/NADH assay

The contents of NAD^+, NADH, and their ratio were measured through an NAD^+/NADH assay kit with WST-8 (Beyotime, Shanghai, China). In brief, the cell lysates were centrifuged and the supernatant

was aspirated. A portion of the supernatant was used as the substrate for the determination of the total amount of NAD^+ and NADH. Another part was heated at 60 °C for 30 min for the assessment of the concentrations of NADH. According to the instructions, the supernatant was successively added with acetate dehydrogenase working solution and chromogenic agent. Following incubation at 37 °C (protected from light), the absorbance was detected at 450 nm optical density for further calculation and analysis.

5.13. Superoxide anion detection

Intracellular superoxide anion levels were detected by the fluorescent probe dihydroethidium (DHE) (Beyotime, Shanghai, China). The stretched cells were rinsed twice with PBS and incubated with 5uM DHE solution at 37 °C for 30 min, followed by trypsin digestion. Subsequently, the fluorescence intensity of the DHE probe was detected by flow cytometry to evaluate the superoxide anion concentrations.

5.14. Mitochondrial membrane potential assay

Following PBS rinses, 1 ml of fresh media was added to the stretched cells. According to the protocols of the mitochondrial membrane potential assay kit with JC-1 (Beyotime, Shanghai, China), 1 ml of JC-1 dyeing working solution was subsequently added and incubated at 37 °C for 20 min. JC-1 staining buffer (1×) was then employed to wash samples twice. Afterwards, they were visualized by immunofluorescence microscopy or quantified with flow cytometry. Notably, due to the special configuration of the amino silicone-bottomed plates, the maximum magnification of fluorescent images was limited to 20×.

5.15. Measurement of ECAR and OCR

The ECAR and OCR of the cells were measured through a Seahorse XF 96 device (Agilent Technologies, CA, USA). Briefly, stretched cells after trypsin digestion were seeded in microtiter plates at 3000 cells/well and incubated overnight with 80 μl of culture medium under different conditions. The following day, microplates were maintained at 37 °C in CO_2-free incubators for 1 h prior to measurement. Subsequently, glucose (10 mM), oligomycin (1 μM), and 2-deoxy-D-glucose (2-DG) (50 mM) were sequentially injected during ECAR detections according to the manufacturer's instructions. Oligomycin (1.5 μM), carbonyl cyanide-*p*-trifluoromethoxyphenylhydrazone (FCCP, 1 μM), and rotenone/antimycotic (Rot/AA, 0.5 μM) were injected successively during OCR detections based on the manufacturer's protocols. Respiratory parameters were recorded and calculated following each injection. The obtained OCR and ECAR values were normalized by cell number.

5.16. Luciferase activity assay

Due to the absence of the regular binding site of PGC-1α to the LDHA promoter in the database, the construction of the LDHA promoter plasmid (Abiotech, Jinan, China) was limited to exclude the mutant plasmid. 293 T cells were inoculated in 24-well plates at 2.5×10^5 cells/well. Following cell attachment, lip2000 was utilized to assist in the transfection of the LDHA promoter plasmid (2 μg/well). After 24 h in culture, cells were virally transfected as described above to overexpress PGC-1α.

The luciferase activities of promoters were assessed by the duo-lite luciferase assay system (Vazyme, Nanjing, China). Briefly, 500ul of duo-lite luciferase reagents were added to the samples and left disrupted at room temperature for 10 min to detect firefly luminescence. Subsequently, the reaction was terminated by 500ul of duo-lite stop & lite reagents. After incubation for another 10 min, renilla luminescence was measured. The promoter luciferase activity was calculated by the ratio of firefly luminescence to renilla luminescence.

5.17. Protein-protein docking

The crystal structures of PGC-1α and LDHA were retrieved from the PDB database. The obtained protein crystals were preprocessed using the protein preparation wizard module of Schrödinger software. Subsequently, the processed proteins were subjected to protein-protein docking. A lower docking score represented a lower free energy of ligand-receptor binding and a higher binding stability. The chains of the interacted protein-protein complexes with the lowest scores were labeled with different colors, following by the supplement of surface to show a 3D view. In addition, the protein interaction analysis module was used to determine the specific binding regions. The scores of different docking sites and the amino acid sequences of the most stable docking site were presented in Additional file 2 and Additional file 3.

5.18. Co-immunoprecipitation

1 ml of pre-cooled IP lysate was added to per dish with 90 %–100 % cell density. The lysate supernatant after centrifugation was collected and divided into three parts. One part of the protein solution was subjected to sonication and denaturation according to the western blots procedures. The other two parts were treated with protein A/G magnetic beads (MedChemExpress, Shanghai, China) to pull down proteins bound to IgG and PGC-1α (1:50, 66369–1-lg, Proteintech, Wuhan, China). The obtained immunoprecipitation complexes were further denatured using 1× SDS-PAGE loading buffer. Immunoprecipitated proteins were then analyzed by western blots to determine the binding effect between PGC-1α and LDHA.

5.19. LDH activity assay

According to the manufacturer's procedure of the lactate dehydrogenase assay kit (Nanjing Jiancheng Bioengineering Institute, Nanjing, China), the matrix buffer, coenzyme I working solution, 2,4-dinitrophenylhydrazine, and 0.4 M NaOH solution was successively added to the lysed samples. After adequate reaction, the absorbance based on intracellular LDH activity was detected at 440 nm optical density.

5.20. Establishment of the rat models

Five male Wistar rats (Weitong Lihua Experimental Animal Technology Co. Ltd., Beijing, China) were randomly selected for further treatment. Periodontitis was induced through ligature protocol and LPS injections around the left first mandibular molars of rats for two weeks. Afterwards, the ligature was removed from the affected teeth, followed by supragingival scaling, hydrogen peroxide rinsing, and adjunctive treatments (metronidazole and amoxicillin; Macklin, Shanghai, China) [64]. After a 1-week recovery, 15 g stretched force was applied to the affected and contralateral first molars by nickel-titanium coiled springs (TOMY, Fukushima, Japan) for 7 days as previously reported [65].

5.21. Micro-CT scanning

The harvested rat mandibles were fixed with 4 % paraformaldehyde for 24 h and immersed in 75 % ethanol solution prior to microCT (Quantum GX2, PerkinElmer, Shelton, Connecticut, USA) scanning. The scanning settings were performed using standard acquisition protocols (90 kV, 88 μA, and 72 μM voxel size). Data analysis was calculated by CTAn (Skyscan, Bruker, Billerica, MA, USA) to evaluate the bone volume fraction, trabecular number, trabecular thickness, and trabecular pattern factor levels on the tension side of the first molar.

5.22. Staining of rat tissue sections

Mandibles with rat molars were decalcified, embedded, cut, and deparaffinized sequentially. The obtained tissue sections (5-μm thick)

were stained as the following described.

5.22.1. HE staining

HE staining was conducted according to the HE staining kit (Solarbio, Beijing, China). The tissue sections were successively stained with hematoxylin for 2 min, differentiated in differentiation solution for 5 s, and dealt with eosin for 2 min. After rinsing with distilled water for 5 min, slices were gradient dehydrated and sealed with neutral gum.

5.22.2. TRAP staining

Tissue sections were immersed in 1 M Tris-HCl (pH 9.0) at 37 °C for 1 h. Subsequently, TRAP dye (JoyTech Biology, Shanghai, China) was added dropwise to tissue blocks, and the slices were kept at 37 °C for 10–60 min until regions containing active TRAP on the pressure side were stained red. The nuclear counterstaining was performed with hematoxylin. After water rinsing, the slices were left to air dry and sealed with neutral gum.

5.22.3. Masson staining

Masson staining of mandible tissues was conducted according to the instructions of the modified Masson's trichrome stain kit (Solarbio, Beijing, China). The slices were sequentially reacted with Masson dye following the order of regents. After adequate reaction and water rinsing, slices were gradient dehydrated and sealed.

5.22.4. Immunohistochemistry staining

Sodium citrate solution was utilized to immerse the dewaxed slices for antigenic thermal repair. The slices were successively reacted with 3 % hydrogen peroxide solution for 15 min, blocked with goat serum for 1 h, and incubated with the following antibodies at 4 °C overnight: anti-ALP (1:100, SA40–00, HuaBio, Hangzhou, China) and anti-PGC-1α (1:50, 66369–1-lg, Proteintech, Wuhan, China). The next day, staining was visualized through DAB working solution for 10 s, followed by counterstaining with hematoxylin for 2 min. The level of antigen expression was quantified through ImageJ.

5.23. Statistical analysis

All collected data obeyed normal distribution and was presented as mean ± standard deviation (SD). Statistical analysis was performed via GraphPad Prism 9.0 (GraphPad Software Inc., San Diego, USA). The comparison between two groups was conducted using Student's *t*-test. The calculation from three or more groups was determined with one-way analysis of variance (ANOVA). A significance level of $P < 0.05$ was accepted. The exhibited error bars denoted SD of at least three replicates unless indicated.

Supplementary data to this article can be found online at https://doi.org/10.1016/j.bone.2024.117132.

Ethics approval and consent to participate

All experiments involving human tissues in this study were approved by the Medical Ethical Committee at the School of Stomatology, Shandong University (No. 20210140; Approval date: 29 January 2021) and was performed in accordance with Helsinki Declaration. Informed consent was obtained from all individual participants or their legal guardians included in the study. All animal experiments conducted in this study were granted approval by the Committee on the Ethics of Animal Experiments of Shandong University (No. 20200709; Approval date: 29 July 2020) and were carried out in strict adherence to the principles outlined in the Basel Declaration.

Funding

This work was supported by the National Natural Science Foundation of China (No. 82071080), the Fundamental Research Funds for the Central Universities (No. 2022JC017) and Academician Laboratory of Immune and Oral Development & Regeneration, Dalian Medical University (No. 2021002).

CRediT authorship contribution statement

Jiani Liu: Writing – original draft, Writing – review & editing, Conceptualization, Methodology, Validation, Formal analysis, Investigation, Data curation, Visualization. **Jixiao Wang:** Writing – review & editing, Methodology, Investigation, Data curation. **Ziyao Wang:** Methodology, Formal analysis, Data curation. **Huiying Ren:** Methodology, Investigation, Formal analysis, Data curation. **Zijie Zhang:** Writing – review & editing, Conceptualization. **Yajing Fu:** Writing – review & editing. **Lan Li:** Writing – review & editing, Conceptualization. **Zhiyuan Shen:** Methodology. **Tianyi Li:** Writing – original draft, Visualization, Validation, Software, Methodology, Investigation, Formal analysis, Data curation. **Shuai Tang:** Investigation. **Fulan Wei:** Writing – review & editing, Supervision, Project administration, Funding acquisition.

Declaration of competing interest

The authors declare that they have no known competing financial interests or personal relationships that could have appeared to influence the work reported in this paper.

Data availability

The datasets used and analyzed during the current study are available from the corresponding author upon reasonable request.

Acknowledgments

We would like to thank Xiaolu Zhao, Fenglu Zhao, Bowen Zhang and Yiling Meng for their assistance with animal studies. We also acknowledge Yixuan Li, Chen Cheng and Mingrui Zhai for their help with culturing primary cells.

References

[1] S. Rayego-Mateos, R.R. Rodrigues-Diez, B. Fernandez-Fernandez, C. Mora-Fernández, V. Marchant, J. Donate-Correa, J.F. Navarro-González, A. Ortiz, M. Ruiz-Ortega, Targeting inflammation to treat diabetic kidney disease: the road to 2030, Kidney Int. 103 (2) (2023) 282–296.
[2] A. Low, E. Mak, J.B. Rowe, H.S. Markus, J.T. O'Brien, Inflammation and cerebral small vessel disease: a systematic review, Ageing Res. Rev. 53 (2019) 100916.
[3] M. Mack, Inflammation and fibrosis, Matrix Biology: journal of the International Society for Matrix Biology 68-69 (2018) 106–121.
[4] Z. Zhao, Y. Li, M. Wang, S. Zhao, Z. Zhao, J. Fang, Mechanotransduction pathways in the regulation of cartilage chondrocyte homoeostasis, J. Cell. Mol. Med. 24 (10) (2020) 5408–5419.
[5] F. Stapleton, M. Bakkar, N. Carnt, R. Chalmers, A.K. Vijay, S. Marasini, A. Ng, J. Tan, H. Wagner, C. Woods, J.S. Wolffsohn, CLEAR - Contact lens complications, Contact lens & anterior eye: the journal of the British Contact Lens Association 44 (2) (2021) 330–367.
[6] F. Wei, X. Xu, C. Zhang, Y. Liao, B. Ji, N. Wang, Stress fiber anisotropy contributes to force-mode dependent chromatin stretching and gene upregulation in living cells, Nat. Commun. 11 (1) (2020) 4902.
[7] J. Liu, Q. Li, S. Liu, J. Gao, W. Qin, Y. Song, Z. Jin, Periodontal ligament stem cells in the periodontitis microenvironment are sensitive to static mechanical strain, Stem Cells Int. 2017 (2017) 1380851.
[8] Y.A. Miroshnikova, S.A. Wickström, Mechanical forces in nuclear organization, Cold Spring Harb. Perspect. Biol. 14 (1) (2022).
[9] Y. Lai, Y. Huang, Mechanisms of mechanical force induced pulmonary vascular endothelial hyperpermeability, Front. Physiol. 12 (2021) 714064.
[10] S.A.U. Shinge, D. Zhang, A.U. Din, F. Yu, Y. Nie, Emerging Piezo1 signaling in inflammation and atherosclerosis; a potential therapeutic target, Int. J. Biol. Sci. 18 (3) (2022) 923–941.
[11] E. Felli, S. Selicean, S. Guixé-Muntet, C. Wang, J. Bosch, A. Berzigotti, J. Gracia-Sancho, Mechanobiology of portal hypertension, JHEP reports: innovation in hepatology 5 (11) (2023) 100869.
[12] J. Yan, L. Zhang, L. Li, W. He, W. Liu, Developmentally engineered bio-assemblies releasing neurotrophic exosomes guide in situ neuroplasticity following spinal cord injury, Materials today. Bio 16 (2022) 100406.

[13] A.F. McGettrick, L.A.J. O'Neill, The role of HIF in immunity and inflammation, Cell Metab. 32 (4) (2020) 524–536.
[14] C. Bao, S. Zhu, K. Song, C. He, HK2: a potential regulator of osteoarthritis via glycolytic and non-glycolytic pathways, Cell communication and signaling: CCS 20 (1) (2022) 132.
[15] Z. Zhang, S. Cui, Y. Fu, J. Wang, J. Liu, F. Wei, Mechanical force induces mitophagy-mediated anaerobic oxidation in periodontal ligament stem cells, Cell. Mol. Biol. Lett. 28 (1) (2023) 57.
[16] R. Santos, L. Lokmane, D. Ozdemir, C. Traoré, A. Agesilas, C. Hakibilen, Z. Lenkei, D. Zala, Local glycolysis fuels actomyosin contraction during axonal retraction, J. Cell Biol. 222 (12) (2023).
[17] X. Yang, Q. Jiang, T. Luan, C. Yu, Z. Liu, T. Wang, J. Wan, J. Huang, K. Li, Pyruvate dehydrogenase kinase 1 inhibition mediated oxidative phosphorylation enhancement in cartilage promotes osteoarthritis progression, BMC Musculoskelet. Disord. 24 (1) (2023) 597.
[18] L. Zheng, Z. Zhang, P. Sheng, A. Mobasheri, The role of metabolism in chondrocyte dysfunction and the progression of osteoarthritis, Ageing Res. Rev. 66 (2021) 101249.
[19] T. Ishida, S. Nakao, T. Ueyama, Y. Harada, T. Kawamura, Metabolic remodeling during somatic cell reprogramming to induced pluripotent stem cells: involvement of hypoxia-inducible factor 1, Inflammation and regeneration 40 (2020) 8.
[20] X. Lv, Y. Lv, X. Dai, Lactate, histone lactylation and cancer hallmarks, Expert Rev. Mol. Med. 25 (2023) e7.
[21] F. Gao, T. Liang, Y.W. Lu, X. Fu, X. Dong, L. Pu, T. Hong, Y. Zhou, Y. Zhang, N. Liu, F. Zhang, J. Liu, A.P. Malizia, H. Yu, W. Zhu, D.B. Cowan, H. Chen, X. Hu, J. D. Mably, J. Wang, D.Z. Wang, J. Chen, A defect in mitochondrial protein translation influences mitonuclear communication in the heart, Nat. Commun. 14 (1) (2023) 1595.
[22] W.J. Zhong, T. Liu, H.H. Yang, J.X. Duan, J.T. Yang, X.X. Guan, J.B. Xiong, Y. F. Zhang, C.Y. Zhang, Y. Zhou, C.X. Guan, TREM-1 governs NLRP3 inflammasome activation of macrophages by firing up glycolysis in acute lung injury, Int. J. Biol. Sci. 19 (1) (2023) 242–257.
[23] S. Wang, Y. Zhao, J. Yang, S. Liu, W. Ni, X. Bai, Z. Yang, D. Zhao, M. Liu, Ginseng polysaccharide attenuates red blood cells oxidative stress injury by regulating red blood cells glycolysis and liver gluconeogenesis, J. Ethnopharmacol. 300 (2023) 115716.
[24] K.L. Storoschuk, D. Lesiuk, J. Nuttall, M. LeBouedec, A. Khansari, H. Islam, B. J. Gurd, Impact of fasting on the AMPK and PGC-1α axis in rodent and human skeletal muscle: a systematic review, Metab. Clin. Exp. 155768 (2023).
[25] O. Abu Shelbayeh, T. Arroum, S. Morris, K.B. Busch, PGC-1α Is a Master Regulator of Mitochondrial Lifecycle and ROS Stress Response, Antioxidants (Basel, Switzerland) 12(5), 2023.
[26] C. Martin, B. Celis, N. Ambrosio, J. Bollain, G.N. Antonoglou, E. Figuero, Effect of orthodontic therapy in periodontitis and non-periodontitis patients: a systematic review with meta-analysis, J. Clin. Periodontol. 49 (Suppl. 24) (2022) 72–101.
[27] X. Zhou, X. Luan, Z. Chen, M. Francis, G. Gopinathan, W. Li, X. Lu, S. Li, C. Wu, T. G. Diekwisch, MicroRNA-138 inhibits periodontal progenitor differentiation under inflammatory conditions, J. Dent. Res. 95 (2) (2016) 230–237.
[28] M. Zhai, S. Cui, L. Li, C. Cheng, Z. Zhang, J. Liu, F. Wei, Mechanical force modulates alveolar bone marrow mesenchymal cells characteristics for bone remodeling during orthodontic tooth movement through lactate production, Cells 11 (23) (2022).
[29] L. Li, W. Liu, H. Wang, Q. Yang, L. Zhang, F. Jin, Y. Jin, Mutual inhibition between HDAC9 and miR-17 regulates osteogenesis of human periodontal ligament stem cells in inflammatory conditions, Cell Death Dis. 9 (5) (2018) 480.
[30] Y. Huang, Q. Liu, L. Liu, F. Huo, S. Guo, W. Tian, Lipopolysaccharide-preconditioned dental follicle stem cells derived small extracellular vesicles treating periodontitis via reactive oxygen species/mitogen-activated protein kinase signaling-mediated antioxidant effect, Int. J. Nanomedicine 17 (2022) 799–819.
[31] H. Yang, G. Li, N. Han, X. Zhang, Y. Cao, Y. Cao, Z. Fan, Secreted frizzled-related protein 2 promotes the osteo/odontogenic differentiation and paracrine potentials of stem cells from apical papilla under inflammation and hypoxia conditions, Cell Prolif. 53 (1) (2020) e12694.
[32] S.J. Kierans, C.T. Taylor, Regulation of glycolysis by the hypoxia-inducible factor (HIF): implications for cellular physiology, J. Physiol. 599 (1) (2021) 23–37.
[33] M. Ždralević, A. Brand, L. Di Ianni, K. Dettmer, J. Reinders, K. Singer, K. Peter, A. Schnell, C. Bruss, S.M. Decking, G. Koehl, B. Felipe-Abrio, J. Durivault, P. Bayer, M. Evangelista, T. O'Brien, P.J. Oefner, K. Renner, J. Pouysségur, M. Kreutz, Double genetic disruption of lactate dehydrogenases A and B is required to ablate the "Warburg effect" restricting tumor growth to oxidative metabolism, J. Biol. Chem. 293 (41) (2018) 15947–15961.
[34] B.D. Fink, J.A. Herlein, M.A. Yorek, A.M. Fenner, R.J. Kerns, W.I. Sivitz, Bioenergetic effects of mitochondrial-targeted coenzyme Q analogs in endothelial cells, J. Pharmacol. Exp. Ther. 342 (3) (2012) 709–719.
[35] H. Wang, J. Su, M. Yu, Y. Xia, Y. Wei, PGC-1α in osteoarthritic chondrocytes: from mechanism to target of action, Front. Pharmacol. 14 (2023) 1169019.
[36] W. Dai, J. Yang, X. Liu, Q. Mei, W. Peng, X. Hu, Anti-colorectal cancer of Ardisia gigantifolia Stapf. And targets prediction via network pharmacology and molecular docking study, BMC complementary medicine and therapies 23 (1) (2023) 4.
[37] B. Xiao, M.J. Sanders, D. Carmena, N.J. Bright, L.F. Haire, E. Underwood, B. R. Patel, R.B. Heath, P.A. Walker, S. Hallen, F. Giordanetto, S.R. Martin, D. Carling, S.J. Gamblin, Structural basis of AMPK regulation by small molecule activators, Nat. Commun. 4 (2013) 3017.
[38] K.A. Merrick, S. Larochelle, C. Zhang, J.J. Allen, K.M. Shokat, R.P. Fisher, Distinct activation pathways confer cyclin-binding specificity on Cdk1 and Cdk2 in human cells, Mol. Cell 32 (5) (2008) 662–672.
[39] H. Vignes, C. Vagena-Pantoula, J. Vermot, Mechanical control of tissue shape: cell-extrinsic and -intrinsic mechanisms join forces to regulate morphogenesis, Semin. Cell Dev. Biol. 130 (2022) 45–55.
[40] X. Li, X. Wang, C. Zhang, J. Wang, S. Wang, L. Hu, Dysfunction of metabolic activity of bone marrow mesenchymal stem cells in aged mice, Cell Prolif. 55 (3) (2022) e13191.
[41] H. Hu, P. Zhao, J. Liu, Q. Ke, C. Zhang, Y. Guo, H. Ding, Lanthanum phosphate/chitosan scaffolds enhance cytocompatibility and osteogenic efficiency via the Wnt/β-catenin pathway, J. Nanobiotechnol. 16 (1) (2018) 98.
[42] X. Li, B.M. Tian, D.K. Deng, F. Liu, H. Zhou, D.Q. Kong, H.L. Qu, L.J. Sun, X.T. He, F.M. Chen, LncRNA GACAT2 binds with protein PKM1/2 to regulate cell mitochondrial function and cementogenesis in an inflammatory environment, Bone research 10 (1) (2022) 29.
[43] Y. Zhang, M. Fang, Z. Yang, W. Qin, S. Guo, J. Ma, W. Chen, GATA binding protein 4 regulates tooth root dentin development via FBP1, Int. J. Biol. Sci. 16 (1) (2020) 181–193.
[44] C.C. Chou, C.P. Wang, J.H. Chen, H.H. Lin, Anti-Atherosclerotic Effect of Hibiscus Leaf Polyphenols against Tumor Necrosis Factor-Alpha-Induced Abnormal Vascular Smooth Muscle Cell Migration and Proliferation, Antioxidants (Basel, Switzerland) 8(12), 2019.
[45] H. Fang, K. Yang, P. Tang, N. Zhao, R. Ma, X. Luo, Q. Liu, Glycosylation end products mediate damage and apoptosis of periodontal ligament stem cells induced by the JNK-mitochondrial pathway, Aging 12 (13) (2020) 12850–12868.
[46] B. Rath-Deschner, A.V.B. Nogueira, S. Beisel-Memmert, M. Nokhbehsaim, S. Eick, J.A. Cirelli, J. Deschner, A. Jäger, A. Damanaki, Interaction of periodontitis and orthodontic tooth movement-an in vitro and in vivo study, Clin. Oral Investig. 26 (1) (2022) 171–181.
[47] B. Li, Y. Shi, M. Liu, F. Wu, X. Hu, F. Yu, C. Wang, L. Ye, Attenuates of NAD(+) impair BMSC osteogenesis and fracture repair through OXPHOS, Stem Cell Res Ther 13 (1) (2022) 77.
[48] W.Q. Ma, X.J. Sun, Y. Zhu, N.F. Liu, PDK4 promotes vascular calcification by interfering with autophagic activity and metabolic reprogramming, Cell Death Dis. 11 (11) (2020) 991.
[49] V. Jacquier, D. Gitenay, S. Fritsch, S. Bonnet, B. Győrffy, S. Jalaguier, L.K. Linares, V. Cavaillès, C. Teyssier, RIP140 inhibits glycolysis-dependent proliferation of breast cancer cells by regulating GLUT3 expression through transcriptional crosstalk between hypoxia induced factor and p53, Cellular and molecular life sciences: CMLS 79 (5) (2022) 270.
[50] O. Yi, Y. Lin, M. Hu, S. Hu, Z. Su, J. Liao, B. Liu, L. Liu, X. Cai, Lactate metabolism in rheumatoid arthritis: pathogenic mechanisms and therapeutic intervention with natural compounds, Phytomedicine: international journal of phytotherapy and phytopharmacology 100 (2022) 154048.
[51] C. Raggi, M.L. Taddei, E. Sacco, N. Navari, M. Correnti, B. Piombanti, M. Pastore, C. Campani, E. Pranzini, J. Iorio, G. Lori, T. Lottini, C. Peano, J. Cibella, M. Lewinska, J.B. Andersen, L. di Tommaso, L. Viganò, G. Di Maira, S. Madiai, M. Ramazzotti, I. Orlandi, A. Arcangeli, P. Chiarugi, F. Marra, Mitochondrial oxidative metabolism contributes to a cancer stem cell phenotype in cholangiocarcinoma, J. Hepatol. 74 (6) (2021) 1373–1385.
[52] X. Zhang, F. Gao, Exercise improves vascular health: role of mitochondria, Free Radic. Biol. Med. 177 (2021) 347–359.
[53] I. Suntar, A. Sureda, T. Belwal, A. Sanches Silva, R.A. Vacca, D. Tewari, E. Sobarzo-Sánchez, S.F. Nabavi, S. Shirooie, A.R. Dehpour, S. Xu, B. Yousefi, M. Majidinia, M. Daglia, G. D'Antona, S.M. Nabavi, Natural products, PGC-1 α, and Duchenne muscular dystrophy, Acta Pharm. Sin. B 10 (5) (2020) 734–745.
[54] T. Zehnder, F. Petrelli, J. Romanos, E.C. De Oliveira Figueiredo, T.L. Lewis Jr., N. Déglon, F. Polleux, M. Santello, P. Bezzi, Mitochondrial biogenesis in developing astrocytes regulates astrocyte maturation and synapse formation, Cell Rep. 35 (2) (2021) 108952.
[55] Y. Zhao, J. Zhang, Y. Zheng, Y. Zhang, X.J. Zhang, H. Wang, Y. Du, J. Guan, X. Wang, J. Fu, NAD(+) improves cognitive function and reduces neuroinflammation by ameliorating mitochondrial damage and decreasing ROS production in chronic cerebral hypoperfusion models through Sirt1/PGC-1α pathway, J. Neuroinflammation 18 (1) (2021) 207.
[56] X. Qin, M. Jiang, Y. Zhao, J. Gong, H. Su, F. Yuan, K. Fang, X. Yuan, X. Yu, H. Dong, F. Lu, Berberine protects against diabetic kidney disease via promoting PGC-1α-regulated mitochondrial energy homeostasis, Br. J. Pharmacol. 177 (16) (2020) 3646–3661.
[57] J. Sun, F.H. Song, J.Y. Wu, L.Q. Zhang, D.Y. Li, S.J. Gao, D.Q. Liu, Y.Q. Zhou, W. Mei, Sestrin2 overexpression attenuates osteoarthritis pain via induction of AMPK/PGC-1α-mediated mitochondrial biogenesis and suppression of neuroinflammation, Brain Behav. Immun. 102 (2022) 53–70.
[58] F.S. Wang, R.W. Wu, Y.S. Chen, J.Y. Ko, H. Jahr, W.S. Lian, Biophysical Modulation of the Mitochondrial Metabolism and Redox in Bone Homeostasis and Osteoporosis: How Biophysics Converts into Bioenergetics, Antioxidants (Basel, Switzerland) 10(9), 2021.
[59] Q. Zhou, H. Xu, L. Yan, L. Ye, X. Zhang, B. Tan, Q. Yi, J. Tian, J. Zhu, PGC-1α promotes mitochondrial respiration and biogenesis during the differentiation of hiPSCs into cardiomyocytes, Genes & diseases 8 (6) (2021) 891–906.
[60] J.A. Villena, New insights into PGC-1 coactivators: redefining their role in the regulation of mitochondrial function and beyond, FEBS J. 282 (4) (2015) 647–672.
[61] G.A. Brooks, C.C. Curl, R.G. Leija, A.D. Osmond, J.J. Duong, J.A. Arevalo, Tracing the lactate shuttle to the mitochondrial reticulum, Exp. Mol. Med. 54 (9) (2022) 1332–1347.
[62] Y. Li, Q. Zhan, M. Bao, J. Yi, Y. Li, Biomechanical and biological responses of periodontium in orthodontic tooth movement: up-date in a new decade, Int. J. Oral Sci. 13 (1) (2021) 20.

[63] J. Liu, H. Wang, L. Zhang, X. Li, X. Ding, G. Ding, F. Wei, Periodontal ligament stem cells promote polarization of M2 macrophages, J. Leukoc. Biol. 111 (6) (2022) 1185–1197.
[64] M. Feres, B. Retamal-Valdes, M.J. Mestnik, L.C. de Figueiredo, M. Faveri, P. M. Duarte, A. Fritoli, E. Faustino, M.L.S. Souto, M. de Franco Rodrigues, M. Giudicissi, B.C.L. Nogueira, L. Saraiva, G.A. Romito, C.M. Pannuti, The ideal time of systemic metronidazole and amoxicillin administration in the treatment of severe periodontitis: study protocol for a randomized controlled trial, Trials 19 (1) (2018) 201.
[65] J. Wang, H. Yang, X. Ma, J. Liu, L. Li, L. Chen, F. Wei, LRP6/filamentous-actin signaling facilitates osteogenic commitment in mechanically induced periodontal ligament stem cells, Cell. Mol. Biol. Lett. 28 (1) (2023) 7.